Theoretical analysis of mixing in liquid clouds. Part 3: Inhomogeneous mixing

M. Pinsky(1), A. Khain(1), and A. Korolev(2)

(1) Department of Atmospheric Sciences, The Hebrew University of Jerusalem, Israel

(2) Environment Canada, Cloud Physics and Severe Weather Section, Toronto, Canada

Submitted to

Atmospheric Chemistry and Physics

Revised

April 2016

Communicating author: Alexander Khain, The Hebrew University of Jerusalem, khain@vms.huji.ac.il

Abstract

An idealized diffusion-evaporation model of time-dependent mixing between a cloud volume and a droplet-free volume is analyzed. The initial droplet size distribution (DSD) in the cloud volume is assumed to be monodisperse. It is shown that evolution of the microphysical variables and the final equilibrium state are unambiguously determined by two non-dimensional parameters. The first one is the potential evaporation parameter R, proportional to the ratio of the saturation deficit to the liquid water content in the cloud volume, that determines whether the equilibrium state is reached at 100% relative humidity, or is characterized by a complete evaporation of cloud droplets. The second parameter Da is the *Damkölher* number equal to the ratio of the characteristic mixing time to the phase relaxation time. Parameters R and Da determine the type of mixing.

The results are analyzed within a wide range of values of R and Da. It is shown that there is no pure homogeneous mixing, since the first mixing stage is always inhomogeneous. The mixing type can change during the mixing process. Any mixing type leads to formation of a tail of small droplets in DSD and, therefore, to DSD broadening that depends on Da. At large Da, the final DSD dispersion can be as large as 0.2. The total duration of mixing varies from several to one hundred phase relaxation time periods, depending on R and Da.

The definitions of homogeneous and inhomogeneous types of mixing are reconsidered and clarified, enabling a more precise delimitation between them. The paper also compares the results obtained with those based on the classic mixing concepts.

Keywords: homogeneous and inhomogeneous mixing, turbulent diffusion, droplet evaporation

1. Introduction

Cloud physics typically investigates two types of turbulent mixing: homogeneous and extremely inhomogeneous (e.g. Burner and Brenguier, 2006; Andrejczuk et al., 2009; Devenish et al., 2012; Kumar et al., 2012). The concept of extremely inhomogeneous mixing in clouds was introduced by Latham and Reed (1977); Baker and Latham (1979), Baker et al. (1980) and Blyth et al. (1980). According to this concept, mixing of cloud air and sub-saturated air from cloud surrounding results in complete evaporation of a fraction of cloud droplets, whereas size of other droplets remain unchanged. The studies of extremely inhomogeneous mixing were closely related to investigation of different mechanisms underlying enhanced growth of cloud droplets and warm precipitation formation (Baker et al., 1980; Baker and Latham, 1982). The concept of homogeneous mixing suggests that all the droplets partially evaporate, so the liquid water content decreases while the droplet concentration remains unchanged (Lehmann et al., 2009; Pt1). The significance of the concepts of homogeneous and inhomogeneous mixing goes far beyond formation of large-sized droplets. In fact, these concepts are closely related to the mechanisms involved in formation of droplet size distributions (DSD) in clouds and to the description of this formation in numerical cloud models. A detailed analysis of the classical concepts of homogeneous and extremely inhomogeneous mixing is given by Korolev et al. (2016, hereafter Pt1).

Mixing in clouds includes two processes: mechanical mixing caused by turbulent diffusion and droplet evaporation accompanied by increasing relative humidity. The relative contribution of these processes can be evaluated by comparison of two characteristic time scales: the characteristic mixing time scale $\tau_{mix} \sim L^{2/3}\varepsilon^{-1/3}$ (where L is the characteristic linear scale of an entrained volume and ε is the dissipation rate of turbulent kinetic energy) and the time of phase relaxation $\tau_{pr} = \left(4\pi \mathscr{D} \overline{r} N\right)^{-1}$ (where N is droplet concentration in a cloud volume, $\overline{r}$ is the mean droplet radius and $\mathscr{D}$ is the diffusivity of water vapor) characterizing the response of the droplet population to changes in humidity (the list of notations is given in Appendix). The

choice of the phase relaxation time as the characteristic time scale of mixing is discussed by Pinsky et al. (2016) (hereafter referred to as Pt. 2) and will be further elaborated below.

Mixing is considered homogeneous if $\tau_{mix} / \tau_{pr} << 1$. At the first stage of mixing, the initial gradients of the microphysical and thermodynamic variables rapidly decrease to zero. By the end of this stage, the fields of temperature, humidity (hence, the relative humidity, RH) and droplet concentration are spatially homogenized and all the droplets within the mixing volume experience the same saturation deficit. During the relatively lengthy second stage, droplets evaporate and increase the relative humidity in the volume. It was shown that homogeneous mixing takes place at scales below about 0.5 m (Pt. 2)

At spatial scales larger than ~0.5 m, $\tau_{mix} / \tau_{pr} > 1$ and the spatial gradients of RH remain for a long time. Consequently, droplets within the mixing volume experience different subsaturations, thus the mixing is considered inhomogeneous. At $\tau_{mix} / \tau_{pr} >> 1$, the mixing is considered extremely inhomogeneous.

According to the classical conceptual scheme, during the first stage of extremely inhomogeneous mixing a fraction of droplets is transported into the droplet-free entrained volume and evaporates completely. The evaporation continues until the evaporating droplets saturate the initially droplet-free volume. At the second stage, turbulent mixing between the cloud volume and the initially droplet-free (but already saturated) volume homogenizes the gradients of droplet concentration and other quantities. Since both volumes are saturated, mixing does not affect droplet sizes. As a result, the final (equilibrium) state is characterized by the relative humidity RH=100% and the DSD shape similar to that before mixing, but with a lower droplet concentration. The same result (a decrease in droplet concentration but unchanged droplet size) is expected in cases of both monodisperse and polydisperse initial DSD. Since the DSD shape does not change, the characteristic droplet sizes (i.e. the mean

square radius, the mean volume radius and the effective radius) do not change either in the course of extremely inhomogeneous mixing.

Thus, according to the classical concepts, the final equilibrium state with RH=100% is reached either by a partial evaporation of all droplets (homogeneous mixing) or a total evaporation of a certain portion of droplets that does not affect the remaining droplets (extremely inhomogeneous mixing) (Lehmann et al., 2009; Pt1).

In analyses of in-situ measurements, the observed data are usually compared with those expected at the final state of mixing as assumed by the classical mixing concepts. If droplet concentration decreases without a corresponding change in the characteristic droplet radius, the mixing is considered "extremely inhomogeneous." If the characteristic droplet radius decreases with an increase of the dilution level while droplet concentration decreases insignificantly, the mixing is identified as "homogeneous." If both the characteristic droplet radius and the droplet concentration change, the mixing is considered as "intermediate". Quantitative evaluations of the microphysical processes specific for intermediate mixing remain largely uncertain.

As was discussed in Pt 2, the final states of mixing suggested by the classical concepts are only hypothetical. To understand the essence of the final equilibrium states of mixing and evaluate the time needed to reach them, it is necessary to consider the time evolution of DSD in the course of mixing process. Time-dependent process of homogeneous mixing was analyzed in Pt. 2. It was shown that in important cases of wide polydisperse initial DSDs, the final state substantially differs from that hypothesized by the classical concepts.

In this study, which is a Pt 3 of the set of studies, we analyze the time-dependent process of inhomogeneous mixing. The structure of the paper is as follows. The main concept and the basic equations for time-dependent inhomogeneous mixing are described in Section 2. Analysis of non-dimensional diffusion-evaporation equations is presented in Section 3. The design and the results of simulations of non-homogeneous mixing are outlined in Sections 4 and 5. A

126 discussion clarifying the concepts of homogeneous and inhomogeneous mixing is presented in
127 concluding Section 6.

128

129 **2. The main concept and the basic equations**

130 During mixing of cloud volume and entrained air volume, the following two processes
131 determine the change of the microphysical and thermodynamical variables: turbulent diffusion
132 resulting in mechanical smoothening of the gradients of temperature, water vapor and droplet
133 concentration, and droplet evaporation accompanied by phase transformation. In this study,
134 inhomogeneous mixing is investigated based on the analysis and solution of a 1D diffusion-
135 evaporation equation. To our knowledge, the idea of using a diffusive model of turbulent
136 mixing to describe the mixing process was first proposed by Baker and Latham (1982). A
137 diffusion-evaporation equation was also analyzed by Jeffery and Reisner (2006). In order to get
138 a more precise understanding of the physics of mixing process the analysis is performed under
139 the following main simplifying assumptions:

140 a) turbulent mixing is analyzed neglecting vertical motions of mixing volumes, droplet
141 collisions and droplet sedimentation.

142 b) the total mixing volume is assumed adiabatic.

143 c) mixing is assumed to take place only along the x-direction, i.e. a 1D task is considered;

144 d) the initial DSD in the cloud volume is assumed monodisperse.

145 Other assumptions and simplifications are discussed below.

146

147 A schematic illustration of the initial conditions used in the study is shown in **Figure 1**.
148 Two air volumes are assumed to mix: a cloud volume (left) and a droplet-free volume (right),
149 each having the linear size of $L/2$. The value of L is assumed within the range of several tens
150 to a few hundred meters. The mixing starts at $t = 0$. The cloud volume is initially saturated
151 $S_1 = 0$, the initial droplet concentration is N_1 and the initial liquid water mixing ratio is

$q_1 = \frac{4\pi\rho_w}{3\rho_a} N_1 r_0^3$. In the droplet-free volume the initial conditions are $RH_2 < 100\%$ (i.e. $S_2 < 0$), $N_2 = 0$ and $q_2 = 0$. Therefore, the initial profiles of these quantities along the x-axis are step functions

$$N(x,0) = \begin{cases} N_1 & \text{if} \quad 0 \le x < L/2 \\ 0 & \text{if} \quad L/2 \le x < L \end{cases} \tag{1a}$$

$$S(x,0) = \begin{cases} 0 & \text{if} \quad 0 \le x < L/2 \\ S_2 & \text{if} \quad L/2 \le x < L \end{cases} \tag{1b}$$

$$q(x,0) = \begin{cases} q_1 & \text{if} \quad 0 \le x < L/2 \\ 0 & \text{if} \quad L/2 \le x < L \end{cases} \tag{1c}$$

The initial profile of droplet concentration is shown in Fig. 1. In this study, averaged equations are used. We do not consider mixing at scales below several millimeters. At the scales of averaging, there exist clear definitions of droplet concentration, supersaturation and other "macro scale" quantities. The mixing is assumed to be driven by isotropic turbulence within the inertial sub-range where the Richardson's law is valid. Accordingly, turbulent diffusion (turbulent mixing) is described by a 1D equation of turbulent diffusion with a turbulent coefficient K. The turbulent coefficient is evaluated as proposed by Monin and Yaglom (1975)

$$K(L) = C\varepsilon^{1/3} L^{4/3} \tag{2}$$

In Eq. (2), C is a constant. Eq. (2) is valid in case turbulent diffusion is considered, i.e. at scales where molecular diffusion can be neglected.

Since the total mixing volume is adiabatic, the fluxes of different quantities through the left and right boundaries of the volume are equal to zero at any time instance, i.e.

$$\frac{\partial N(0,t)}{\partial x} = \frac{\partial N(L,t)}{\partial x} = 0; \quad \frac{\partial q(0,t)}{\partial x} = \frac{\partial q(L,t)}{\partial x} = 0; \frac{\partial q_v(0,t)}{\partial x} = \frac{\partial q_v(L,t)}{\partial x} = 0 \tag{3}$$

where q_v is the water vapor mixing ratio.

During mixing, droplets in the mixing volume experience different subsaturations, therefore, the initially monodisperse DSD will become polydisperse. The droplets that were

transported into the initially droplet-free volume will undergo either partial or complete evaporation. The evaporation leads to a decrease in both droplet size and droplet concentration.

The basic system of equations that describes the processes of diffusion and of evaporation which occur simultaneously is to be derived. The first equation is written for value Γ defined as

$$\Gamma = S + A_2 q \tag{4}$$

This value is conservative in a moist adiabatic process, i.e. it does not change during phase transitions (Pinsky et al., 2013, 2014). In Eq. (4), the coefficient $A_2 = \frac{1}{q_v} + \frac{L_w^2}{c_p R_v T^2}$ is a weak function of temperature that changes by ~10 % when temperatures change by ~10 ^{o}C (Pinsky et al., 2013). In this study, it is assumed that $A_2 = constant$. In Eq. (4), $q = \frac{4\pi\rho_w}{3\rho_a}\int_0^\infty r^3 f(r)dr$ is the liquid water mixing ratio and $f(r)$ is the DSD. The quantity Γ obeys the diffusion equation

$$\frac{\partial\Gamma(x,t)}{\partial t} = K\frac{\partial^2\Gamma(x,t)}{\partial x^2} \tag{5}$$

with the boundary conditions $\frac{\partial\Gamma(0,t)}{\partial x} = \frac{\partial\Gamma(L,t)}{\partial x} = 0$ and the initial profile at $t = 0$

$$\Gamma(x,0) = \begin{cases} A_2 q_1 & \text{if} \quad 0 \le x < L/2 \\ \mathrm{S}_2 & \text{if} \quad L/2 \le x < L \end{cases} \tag{6}$$

Therefore, function $\Gamma(x,0)$ is positive in the left volume, and negative in the right volume.

Since Γ does not depend on phase transitions, Eq. (5) can be solved independently of other equations. The solution of Eq. (5) with initial conditions (6) is (Polyanin and Zaitsev, 2004)

$$\Gamma(x,t) = \sum_{n=0}^{\infty} a_n \exp\left(-\frac{Kn^2\pi^2 t}{L^2}\right)\cos\left(\frac{n\pi x}{L}\right) = \frac{1}{2}\left(S_2 + A_2 q_1\right) + (A_2 q_1 - S_2)\sum_{n=1}^{\infty}\frac{\sin(n\pi/2)}{n\pi/2}\exp\left(-\frac{Kn^2\pi^2 t}{L^2}\right)\cos\left(\frac{n\pi x}{L}\right) \tag{7}$$

where the Fourier coefficients of expanding the step function (6) are

$$a_0 = \frac{1}{2}\left(A_2 q_1 + S_2\right) \tag{8a}$$

$$a_n = (A_2 q_1 - S_2)\frac{\sin(n\pi/2)}{n\pi/2},\ n = 1,2,... \tag{8b}$$

An example of spatial dependencies of $\Gamma(x,t)$ at different time instances during the mixing is shown in **Figure 2**. One can see a decrease in the initial gradients and a tendency to establishing a horizontally uniform value of Γ. Since the initial volume was divided into two equal parts, the diffusion leads to formation of a constant limit value of function Γ

$$\Gamma(x,\infty) = \frac{1}{2}\left(\Gamma(0,0) + \Gamma(L,0)\right).$$

The second basic equation is the equation for diffusional droplet growth, taken in the following form (Pruppacher and Klett, 2007)

$$\frac{d\sigma}{dt} = \frac{2S}{F} \tag{9}$$

where $\sigma = r^2$ is the square of droplet radius and $F = \frac{\rho_w L_w^2}{k_a R_v T^2} + \frac{\rho_w R_v T}{e_S(T)\mathscr{D}}$. The value of coefficient F is considered constant in this study. The solution of Eq. (9) is

$$\sigma(t) = \frac{2}{F}\int_0^t S(t')dt' + \sigma_0 \tag{10}$$

The third main equation describes the evolution of DSD. In the following discussion, the DSD will be presented in the form $g(\sigma)$ which is the distribution of the square of the radius. This formulation directly utilizes the property of the diffusion growth equation (9) according to which the time changes of DSD are reduced to shifting the distributions in the space of square radii, while the shape of the distribution remains unchanged. The standard DSD $f(r)$ is related to $g(\sigma)$ as $f(r) = 2r \cdot g(r^2)$.

The normalized condition for $g(\sigma)$ is

$$N = \int_0^\infty g(\sigma) d\sigma \tag{11}$$

where N is the droplet concentration. Using DSD $g(\sigma)$, the liquid water mixing ratio can be presented as integral

$$q = \frac{4\pi\rho_w}{3\rho_a} \int_0^\infty \sigma^{3/2} g(\sigma) d\sigma \tag{12}$$

The 1D diffusion-evaporation equation for the non-conservative function $g(\sigma)$ can be written in the form (Rogers and Yau, 1989)

$$\frac{\partial g(\sigma)}{\partial t} = K \frac{\partial^2 g(\sigma)}{\partial x^2} - \frac{\partial}{\partial \sigma}\left(\frac{d\sigma}{dt} g(\sigma) \right) \tag{13}$$

where the first term on the right-hand side of Eq. (13) describes changes in the DSD due to spatial diffusion, while the second term on the right-hand side describes changes in the DSD due to evaporation. Substitution of Eq. (9) into Eq. (13) leads to the following equation

$$\frac{\partial g(x,t,\sigma)}{\partial t} = K \frac{\partial^2 g(x,t,\sigma)}{\partial x^2} - \frac{2S(x,t)}{F} \frac{\partial g(x,t,\sigma)}{\partial \sigma} \tag{14}$$

To close Eq. (14), Eq. (4) should be used in the form

$$S(x,t) = \Gamma(x,t) - A_2 q(x,t) \tag{15}$$

where $q(x,t)$ is calculated according to Eq. (12). Eqs. (12, 14, 15) constitute a closed set of equations allowing calculation of $g(x,t,\sigma)$.

To proceed to the equations for DSD moments, let us define a moment of DSD $g(\sigma)$ of order α as

$$m_\alpha = \overline{\sigma^\alpha} = \int_0^\infty \sigma^\alpha g(\sigma) d\sigma \tag{16}$$

Multiplying Eq. (14) by σ^α, integrating within limits $[0...\infty]$ and assuming that $\sigma^\alpha g(\sigma) \to 0$ when $\sigma \to \infty$, yield a recurrent formula for the DSD moments

235 $$\frac{\partial m_\alpha(x,t)}{\partial t} = K\frac{\partial^2 m_\alpha(x,t)}{\partial x^2} + \alpha\frac{2S}{F}m_{\alpha-1}(x,t) \quad (17)$$

236 Eq. (17) provides a recurrent relationship between the DSD moments of different orders. This
237 relationship was discussed by Pinsky et al.'s (2014) while analyzing diffusion growth in an
238 ascending adiabatic parcel.

239 In particular, the equation for the liquid water mixing ratio that is a moment of the order of

240 $\alpha = \frac{3}{2}$ can be written as

241 $$\frac{\partial q(x,t)}{\partial t} = K\frac{\partial^2 q(x,t)}{\partial x^2} + \frac{4\pi\rho_w N(x,t)\overline{r}(x,t)}{F\rho_a}S(x,t) \quad (18)$$

242 where the mean radius $\overline{r}(x,t) = \frac{m_{1/2}}{m_0}$.

243 In the general case, Eq. (18) is not closed, since concentration $N(x,t)$ and $\overline{r}(x,t)$ are unknown
244 functions of time and spatial coordinates.

245 The characteristic time of evaporation and of supersaturation change is the phase relaxation
246 time (Korolev and Mazin, 2003)

247 $$\tau_{pr} = \frac{\rho_a F}{4\pi\rho_w A_2 N\overline{r}} \quad (19)$$

248 Using Eq. (19), Eq. (18) can be rewritten as

249 $$\begin{aligned}\frac{\partial q(x,t)}{\partial t} &= K\frac{\partial^2 q(x,t)}{\partial x^2} + \frac{1}{\tau_{pr}(x,t)}\left[\frac{1}{A_2}\Gamma(x,t) - q(x,t)\right] = \\ &= K\frac{\partial^2 q(x,t)}{\partial x^2} + \frac{1}{A_2\tau_{pr}(x,t)}S(x,t)\end{aligned} \quad (20)$$

250 From Eqs. (20) and (15), the equation for supersaturation can be written in the following simple
251 form

252 $$\frac{\partial S(x,t)}{\partial t} = K\frac{\partial^2 S(x,t)}{\partial x^2} - \frac{S(x,t)}{\tau_{pr}(x,t)} \quad (20a)$$

253 Eqs. (20) and (20a) show that changes in the microphysical variables are determined by the rate
254 of spatial diffusion (the first term on the right-hand side of these equations) and of evaporation
255 (the second term on the right-hand side).
256
257 **3. Analysis of non-dimensional equations**
258 Spatial diffusion and evaporation depend on many parameters. It is the best to start the
259 analysis from the basic equation system presented in a non-dimensional form. A time scale
260 corresponding to the initial phase relaxation time in a cloud volume can be defined as

261 $$\tau_0 = \frac{\rho_a F}{4\pi\rho_w A_2 N_1 r_0} \qquad (21)$$

262 and the non-dimensional time is $\tilde{t} = t/\tau_0$. Other non-dimensional parameters to be used are:
263 the non-dimensional phase relaxation time

264 $$\tilde{\tau}_{pr} = \tau_{pr}/\tau_0 = \frac{N_1 r_0}{N(\tilde{x},\tilde{t})\bar{r}(\tilde{x},\tilde{t})}, \qquad (22a),$$

265 the normalized liquid water mixing ratio which is equal to the normalized liquid water content

266 $$\tilde{q} = \frac{q}{q_1}, \qquad (22b),$$

267 the normalized supersaturation

268 $$\tilde{S} = \frac{S}{A_2 q_1} \qquad (22c),$$

269 the non-dimensional conservative function

270 $$\tilde{\Gamma} = \frac{\Gamma}{A_2 q_1} \quad , \qquad (22d),$$

271 the normalized square of droplet radius

272 $$\tilde{\sigma} = \frac{\sigma}{r_0^2}, \qquad (22e),$$

273 the normalized droplet concentration

274 $$\tilde{N} = N/N_1 \qquad (22f)$$

and the non-dimensional DSD

$$\tilde{g}(\tilde{\sigma}) = \frac{r_0^2}{N_1} g(\sigma) \qquad (22g).$$

with normalization $\tilde{N} = \int_0^1 \tilde{g}(\tilde{\sigma}) d\tilde{\sigma}$. The definition (22g) means that the integral of a non-dimensional initial size distribution over the normalized square radius is equal to unity.

The non-dimensional distance and the non-dimensional time are defined as

$$\tilde{x} = x / L; \quad \tilde{t} = t / \tau_0 \qquad (22h)$$

A widely used non-dimensional parameter showing the comparative rates of diffusion and evaporation is the Damkölher number:

$$Da = \frac{\tau_{mix}}{\tau_0} = \frac{L^2}{K \tau_0} \qquad (23)$$

where

$$\tau_{mix} = \frac{L^2}{K} \qquad (24)$$

is the characteristic time scale of mixing. Using the non-dimensional parameters listed above, Eq. (20) can be rewritten in a non-dimensional form as

$$\frac{\partial \tilde{q}(\tilde{x},\tilde{t})}{\partial \tilde{t}} = \frac{1}{Da} \frac{\partial^2 \tilde{q}(\tilde{x},\tilde{t})}{\partial \tilde{x}^2} + \frac{1}{\tilde{\tau}_{pr}(\tilde{x},\tilde{t})} \left[\tilde{\Gamma}(\tilde{x},\tilde{t}) - \tilde{q}(\tilde{x},\tilde{t}) \right] = \frac{1}{Da} \frac{\partial^2 \tilde{q}(\tilde{x},\tilde{t})}{\partial \tilde{x}^2} + \frac{1}{\tilde{\tau}_{pr}(\tilde{x},\tilde{t})} \tilde{S}(\tilde{x},\tilde{t}) \qquad (25)$$

where

$$\tilde{q}(\tilde{x},\tilde{t}) = \frac{N(\tilde{x},\tilde{t}) \overline{\sigma^{3/2}}}{N_1 r_0^3} = \int_0^\infty \tilde{\sigma}^{3/2} \tilde{g}(\tilde{x},\tilde{t},\tilde{\sigma}) d\tilde{\sigma} \qquad (26)$$

The initial conditions and the boundary conditions should be rewritten in a non-dimensional form as well. For instance, the normalized initial condition for the non-dimensional function $\tilde{q}(\tilde{x},0)$ can be derived from Eqs. (1c) and (22b)

$$\tilde{q}(\tilde{x},0)=\begin{cases}1 & \text{if} \quad 0\le\tilde{x}<1/2\\ 0 & \text{if} \quad 1/2\le\tilde{x}<1\end{cases} \tag{27}$$

The solution for $\tilde{\Gamma}(\tilde{x},\tilde{t})$ obtained by a normalization of solution (7) is

$$\tilde{\Gamma}(\tilde{x},\tilde{t})=\frac{1}{2}\left(1+R\right)+\left(1-R\right)\sum_{n=1}^{\infty}\frac{\sin(n\pi/2)}{n\pi/2}\exp\left(-\frac{n^2\pi^2\tilde{t}}{Da}\right)\cos\left(n\pi\tilde{x}\right), \tag{28}$$

where

$$R=\frac{S_2}{A_2q_1} \tag{29}$$

is a non-dimensional parameter referred to, hereafter, as a potential evaporation parameter (PEP). The PEP is proportional to the ratio of the amount of water vapour that should evaporate in order to saturate the initially droplet-free volume (that is determined by S_2) to the initial available liquid water q_1 in the cloud volume. The solution of Eq. (28) at $t\to\infty$ depends only on parameter R.

$$\tilde{\Gamma}(\tilde{x},\infty)=\frac{1}{2}\left(1+R\right) \tag{30}$$

The importance of PEP that determines a possible final state was illustrated in Pt. 1. PEP is also the sole parameter enabling calculation of the normalized mixing diagram for homogeneous mixing (Pt. 2). In this study, we consider cases when $R<0$ since $S_2<0$, i.e. when droplets can only evaporate in the course of mixing.

The solution of Eq. (25) and the type of mixing depends on the values of two non-dimensional parameters, namely, Da and R. Thus, when $R=\frac{S_2}{A_2q_1}<-1$, $\tilde{\Gamma}(\tilde{x},\infty)<0$. It means that the initially droplet-free volume V_2 is too dry and all the droplets in the mixing volume evaporate completely. At the final equilibrium state $RH<100\%$, i.e. $S(x,\infty)<0$. If $R=\frac{S_2}{A_2q_1}>-1$, $\tilde{\Gamma}(\tilde{x},\infty)>0$. This means that the mixed volume in the final state contains droplets, i.e. the mixing leads expands the volume with droplets, i.e. the cloud volume. At the

316 final equilibrium state, $RH = 100\%$ (i.e. $S(x,\infty) = 0$). The case when $|R| = \left|\frac{S_2}{A_2 q_1}\right| = |\tilde{S}_2| << 1$

317 corresponds to either RH close to 100% (i.e. S_2 is close to zero) (this case corresponds to the
318 degenerated case considered in Pt. 1), and/or to the case when the liquid water mixing ratio in
319 the cloud volume is large. In case $|R| << 1$, the second term on the right-hand side of Eq. (25) is
320 much smaller than the first term, and the mixing is driven by turbulent diffusion only.

321 In case $Da \to 0$ (often considered as homogeneous mixing), at the beginning of the mixing
322 the diffusion term is much larger than the evaporation term, the second term on the right-hand
323 side of Eq. (25). As mixing proceeds, within a short time period the total homogenization of all
324 the variables in the mixing volume is established and all the spatial gradients become equal to
325 zero. At this time instance, the first term on the right-hand side becomes equal to zero, and the
326 second term on the right-hand side of Eq. (25), describing droplet evaporation, becomes
327 dominant. Thus, the analysis of the Eq. (25) shows that mixing consists of two stages. The first
328 mixing stage is a short stage of inhomogeneous mixing and the longer second stage of
329 homogeneous mixing. The evolution of the microphysical variables during homogeneous
330 mixing is described in detail in Pt. 2.

331 $Da \to \infty$ corresponds to extremely inhomogeneous mixing, according to the classic
332 concept. In this case, the diffusion term is much smaller than the evaporation term, so
333 evaporation takes place under significant spatial gradients of RH. At $Da = \infty$, the adjacent
334 volumes do not mix at all and remain separated. This equivalent to existence of two
335 independent adiabatic volumes. Another interpretation of the limiting case $Da = \infty$ is an
336 infinite fast droplet evaporation. Both scenarios at $Da \to \infty$ indicate simplifications in the
337 definition of the extremely inhomogeneous mixing. At intermediate values of Da, mixing is
338 inhomogeneous, when both turbulent diffusion and evaporation contribute simultaneously to
339 formation of the DSD.

Using Eq. (14) and normalization (22f), the equations for the non-dimensional size distribution can be written as

$$\frac{\partial \tilde{g}(\tilde{x},\tilde{t},\tilde{\sigma})}{\partial \tilde{t}} = \frac{1}{Da}\frac{\partial^2 \tilde{g}(\tilde{x},\tilde{t},\tilde{\sigma})}{\partial \tilde{x}^2} + \frac{2}{3}\left[\tilde{\Gamma}(\tilde{x},\tilde{t}) - \tilde{q}(\tilde{x},\tilde{t})\right]\frac{\partial \tilde{g}(\tilde{x},\tilde{t},\tilde{\sigma})}{\partial \tilde{\sigma}} \qquad (31)$$

Eq. (31) is solved with the following initial conditions

$$\tilde{g}(\tilde{x},0,\tilde{\sigma}) = \begin{cases} \delta(\tilde{\sigma}-1) & \text{if} \quad 0 \le \tilde{x} < 1/2 \\ 0 & \text{if} \quad 1/2 \le \tilde{x} \le 1 \end{cases} \qquad (32)$$

where $\delta(\tilde{\sigma}-1)$ is a delta function.

Table 1 presents the list of all the non-dimensional variables used in this study and the ranges of their variation. It is shown that six parameters determining the geometrical and microphysical properties of mixing can be reduced to two non-dimensional parameters, which enables a more efficient analysis of mixing. The ranges of parameter variations in Tab. 1 correspond to the simplifications used in the study (the initial DSD is monodisperse and $RH \le 100\%$**).**

4. Design of simulations

Damköller number Da *in clouds*

The characteristic mixing time τ_{mix} can be evaluated using Eqs. (2) and (24)

$$\tau_{mix} = \frac{1}{C}\varepsilon^{-1/3}L^{2/3} \qquad (33)$$

There is significant uncertainty regarding the evaluation of τ_{mix} and Da in clouds, which is largely related to the choice of coefficient C in expression (33). These values differ in different studies: $C = 10$ (Jeffery and Reisner, 2006); $C = 1$ (Lehmann et al., 2009) and $C \approx 0.2$ (Monin and Yaglom, 1975) and Boffetta and Sokolov (2002).

364 According to Lehmann et al. (2009), the values of Da in clouds of different types range
365 from to 0.1 to several hundred. Thus, estimation of Da in clouds may vary within a wide range
366 up to a few orders of magnitude. Da values of in stratocumulus clouds can be similar or even
367 higher than those in cumulus clouds, since both τ_{mix} and τ_{pr} in stratiform clouds are larger than
368 in cumulus clouds.

369 In our simulations, we compare the evolution of the microphysical parameters within a
370 wide range of Da (from 1 up to 500) and of R (from -1.5 up to -0.1). $Da = 1$ represents the
371 case closest to homogeneous mixing, while $Da = 500$ indicates extremely inhomogeneous
372 mixing.

373

374 ***Numerical method***

375 Calculations were performed using MATLAB solver PDEPE. We solve the equation
376 system (31) for normalized DSD $\tilde{g}(\tilde{x},\tilde{t},\tilde{\sigma}_j)$ with the initial condition (32) and the Neumann
377 boundary conditions

378

379 $$\frac{\partial \tilde{g}(0,\tilde{t},\tilde{\sigma}_j)}{\partial \tilde{x}} = \frac{\partial \tilde{g}(1,\tilde{t},\tilde{\sigma}_j)}{\partial \tilde{x}} = 0 \qquad (34)$$

380 where $j = 1...24$ are the bin numbers on a linear grid of square radii. The number of grid points
381 along the $\tilde{x}$ axis was set equal to 81.

382 In calculation of the last term on the right-hand side of Eq. (31), the normalized
383 supersaturation $\tilde{S}$ was calculated first using the normalized conservative equation

384 $$\tilde{S}(\tilde{x},\tilde{t}) = \tilde{\Gamma}(\tilde{x},\tilde{t}) - \tilde{q}(\tilde{x},\tilde{t}) \qquad (35)$$

385 where $\tilde{\Gamma}(\tilde{x},\tilde{t})$ is calculated using Eq. (28). Then, this term was formulated using Eq. (9) as

386 $$\frac{2}{3}\tilde{S}(\tilde{x},\tilde{t})\frac{\partial \tilde{g}(\tilde{x},\tilde{t},\tilde{\sigma}_j)}{\partial \tilde{\sigma}_j} \approx \frac{\tilde{g}\left(\tilde{x},\tilde{t},\tilde{\sigma}_j + \frac{2}{3}\tilde{S}\Delta\tilde{t}\right) - \tilde{g}\left(\tilde{x},\tilde{t},\tilde{\sigma}_j\right)}{\Delta\tilde{t}} \qquad (36)$$

Therefore, at each time step, the DSD $\tilde{g}$ first was shifted to the left to the value $\frac{2}{3}\tilde{S}\Delta\tilde{t}$, where $\Delta\tilde{t}$ is a small time increment chosen so that $\left|\frac{2}{3}\tilde{S}_{\max}\Delta\tilde{t}\right| \le \frac{\Delta\tilde{\sigma}}{2}$. Next, the shifted DSD was remapped onto the fixed square radius grid $\tilde{\sigma}_j$. We used the remapping method proposed by Kovetz and Olund (1969), which conserves droplet concentration and LWC. After remapping, the differences between the new and old DSDs were recalculated. The new values of LWC then were determined using new values of DSD and Eq. (26). MATLAB utility PDEPE automatically chooses the time step needed to provide stability of calculations.

5. Results of simulations

5.1 Full evaporation case

First, we consider the case $R = -1.5$, when all the cloud water evaporates completely. This process corresponds to the cloud dissipation caused by mixing with the entrained dry air. At the final state, RH is expected to be uniform and negative over the entire mixing volume.

Figure 3 shows spatial and time changes of $\tilde{S}$ for $Da = 1$, 50 and 500. At the final state for all the three cases $\tilde{S}$ =-0.25, which is in agreement with the analytical solution of Eq. (30). The final negative value indicates that all the droplets completely evaporated during mixing. At $Da = 1$ (Fig.3ab), two stages of supersaturation evolution can be identified. The first short stage with $t < 0.4\tau_{pr}$ is the period of inhomogeneous mixing, when the gradients of RH persist. By end of the second stage of about $14\tau_{pr}$, the equilibrium state is reached. Thus, at small Da both types of mixing take place. In the cases of $Da = 50$ and $Da = 500$, the spatial gradients exit during the entire period of mixing until the equilibrium state is reached (approximately $50\tau_{pr}$ and $300\tau_{pr}$, respectively) (Fig.3cdef). Therefore, at these Da mixing is inhomogeneous during entire mixing.

410 **Figure 4** shows spatial changes (upper row) and changes in $\tilde{x}-\tilde{t}$ coordinates (lower row)
411 of normalized LWC for the same case as in Fig.3. These diagrams demonstrate a significant
412 difference in the evaporation rates at different Da values. Complete evaporation (LWC=0) is
413 reached at $Da=1$, 50 and 500 by about 12, 22 and 120 relaxation times periods , respectively.

414 Analysis of Figs. 3 and 4 allows to introduce two characteristic time periods: (1) period T_{mix}
415 during which the spatial gradients of the microphysical parameters persist, and mixing is
416 inhomogeneous, and (2) period T_{ev} during which droplet evaporation takes place. Both time
417 periods are dimensionless and normalized using τ_0. Time period T_{ev} is equal either to the time
418 of complete droplet evaporation (when $R<-1.0$) or to the time period during which the
419 saturation deficit in the mixing volume becomes equal to zero (or close to zero if $R>-1.0$),
420 i.e. evaporation is actually terminated. Quantitative evaluations of T_{mix} and T_{ev} will be given in
421 Section 5.3. At $\tilde{t}<T_{mix}$, droplets in the mixing volume experience different saturation deficits.
422 Toward the end of time T_{mix} the saturation deficit becomes uniform over the entire mixing
423 volume because of mechanic mixing. At $Da=1$, the homogenization of the saturation deficit
424 and all the microphysical variables takes place during a very short time of about $0.5\tau_{pr}$, and
425 then the evaporation of droplets is assumed to take place under the same subsaturation
426 conditions, so $T_{mix}<<T_{ev}$.

427 Figs. 4a,b show that at $\tilde{t}\approx 0.35$, normalized LWC drops down from 1 to 0.4. Since the
428 average value of the normalized LWC in the mixing volume is equal to 0.5 (see the initial
429 condition in Eq. (27)), 20% of the droplet mass evaporates during this short inhomogeneous
430 period. Thus, despite being quite short, inhomogeneous mixing stage plays an important role
431 even at $Da=1$.

432 Since at $t=0$ the mixing volume is not spatially homogeneous by definition, there is
433 always a period while spatial inhomogeneity exists. With increasing Da, the duration of the
434 inhomogeneous stage increases and the duration of the homogeneous stage decreases. At

435 $Da = 500$, homogenization of the saturation deficit requires $250\tau_{pr}$, which is twice as long as
436 the time of complete droplet evaporation, i.e. $T_{mix} \approx 2T_{ev}$. This means that at $Da = 500$, droplet
437 evaporation takes place in the presence of the spatial gradients of supersaturation. After
438 complete evaporation of droplets, spatial gradients of the water vapour mixing ratios remain.
439 This kind of mixing is regarded as inhomogeneous.

440 At $Da = 50$, the time of complete evaporation is approximately equal to the time of
441 supersaturation homogenization, i.e. $T_{mix} \approx T_{ev}$. In this case, as at $Da = 500$, the droplets
442 experience different saturation deficit within the mixing volume, so mixing is inhomogeneous
443 at $Da = 50$.

444 The differences in droplet evaporation at different Da can be seen in **Figure 5**., showing
445 the relationships between $\tilde{N}$ and $\tilde{q}$ plotted with a certain time increment, so that each symbol
446 in the diagrams corresponds to a particular time instance. These symbols form curves. Each
447 panel of Fig. 5 shows three curves corresponding to different $\tilde{x}$: the centre of the initially cloud
448 volume ($\tilde{x} = 1/4$); the centre of the mixing volume ($\tilde{x} = 1/2$) and the centre of the initially
449 droplet-free volume ($\tilde{x} = 3/4$). The directions of the time increase are shown by arrows along
450 the corresponding curves. The initial points of the curves corresponding to $\tilde{t} = 0$ are
451 characterized by values $\tilde{q} = 1$ and $\tilde{N} = 1$ at $\tilde{x}$ =1/4, and by values $\tilde{q} = 0$ and $\tilde{N} = 0$ at $\tilde{x} = 3/4$.

452 The behaviour of the $\tilde{N} - \tilde{q}$ relationship provides important information about mixing
453 process. At $\tilde{t} < T_{mix}$, there are spatial gradients of $\tilde{N}$ and $\tilde{q}$, i.e. $\tilde{N}$ and $\tilde{q}$ are different at
454 different $\tilde{x}$. This means that the three curves at $\tilde{t} < T_{mix}$ do not coincide. At $\tilde{t} > T_{mix}$, the spatial
455 gradients of $\tilde{N}$ and $\tilde{q}$ disappear and the three curves coincide. When the curves do not
456 coincide, mixing is inhomogeneous, and the coincidence of the curves indicates that the mixing
457 becomes homogeneous. In Fig. 5a and 5b ($Da = 1$ and $Da = 5$, respectively), the curves
458 coincide at point A corresponding to time $\tilde{t} = T_{mix}$.

459 Figs. 5a,b show that at $Da = 1$ and $Da = 5$, mixing consists of two stages: inhomogeneous
460 and homogeneous. The time instance $\tilde{t} = T_{mix}$ separates these two stages. In turn, the period of
461 homogeneous mixing (when evaporation is spatially homogeneous) can be separated into two
462 sub-periods. During the first sub-period, droplets evaporate only partially and $\tilde{q}$ decreases at
463 the same droplet concentration. This sub-period is very pronounced at $Da = 1$, when $\tilde{q}$
464 decreases from about 0.4 to 0.1 at the unchanged droplet concentration. At the second sub-
465 period, when $\tilde{q} < 0.1$, droplets evaporate completely, beginning with smaller ones, so both the
466 droplet concentration and $\tilde{q}$ rapidly drop to zero. At $Da = 5$ (Fig. 5b), at the stage of
467 homogeneous evaporation (that begins at point "A") the decrease in $\tilde{q}$ is accompanied by a
468 decrease in $\tilde{N}$.

469 At $Da = 50$ (Fig 5c), curves corresponding to different values of $\tilde{x}$ do not coincide, except
470 at the final point "F", where $\tilde{N} = 0$ and $\tilde{q} = 0$. This means that horizontal gradients exist during
471 the entire mixing process and mixing is inhomogeneous till the final equilibrium state is
472 reached. Droplets penetrating into the initially droplet-free volume begin evaporating, so only a
473 small fraction of droplets reaches the centre of the droplet-free volume, as seen in Fig. 5c,
474 $\tilde{x} = 3/4$ (black curve). Accordingly, at $\tilde{x} = 3/4$ the droplet concentrations and $\tilde{q}$ reach their
475 maxima (of 0.1 and 0.05, respectively) and then decrease to zero. At $Da = 500$ (Fig 5d), all
476 the droplets evaporate before reaching the centre of the dry volume, indicating an extremely
477 high spatial inhomogeneity of droplet evaporation. Hence, only two curves for $\tilde{x} = 1/4$ and
478 $\tilde{x} = 1/2$ are seen in Fig.5d.

479 Fig. 5 also shows that the slopes of the curves describing the $\tilde{N} - \tilde{q}$ relationships are
480 different at different values of $\tilde{x}$ and change over time. At large Da, the slopes of the curves
481 describing the dependencies $\tilde{N} - \tilde{q}$ in the initially cloud volume are close to linear. However,
482 the slope at a high value of $\tilde{q}$ is still flatter than that at a low value of $\tilde{q}$. This can be attributed
483 to the fact that when $\tilde{q}$ is large, it decreases faster than the concentration $\tilde{N}$ because some

484 fraction of droplets evaporate only partially. At the end of the mixing when $\tilde{q}$ is small, $\tilde{N}$
485 decreases faster than $\tilde{q}$, because the droplet concentration is determined by the smallest
486 droplets, while $\tilde{q}$ is determined by larger droplets.

487 As was discussed in Pt. 1, according to the classical concept of extremely inhomogeneous
488 mixing, the ratio q/N remains constant. For dimensionless $\tilde{N}$ and $\tilde{q}$, the scattering points
489 should be aligned along the 1:1 line. Therefore, the closeness of particular cases to the classical
490 extremely inhomogeneous mixing can be evaluated by the deviation of the $\tilde{N}-\tilde{q}$ curve from
491 the 1:1 line. One can see that at $Da=500$ the $\tilde{N}-\tilde{q}$ relationship is closer to linear.

492 Despite the fact that at $R<-1$ all the droplets within the mixing volume evaporate, it is
493 interesting to follow the DSD evolution during this process. **Figure 6** shows the time evolution
494 of a normalized DSD at $Da=1$ and $Da=50$. One can see a substantial difference in the DSD
495 evolutions at different Da. At $Da=1$, different DSDs are formed very rapidly at different
496 values of $\tilde{x}$ (panel a). The widest DSD occurs at $\tilde{x}=1$, i.e. at the outer boundary of the initially
497 droplet-free volume. This is natural, because the supersaturation deficit is the highest at $\tilde{x}=1$.
498 At $\tilde{t}>T_{mix}\approx 0.4$, DSD become similar at all values of $\tilde{x}$ (Fig.6b). The DSD width continues to
499 increase due to partial droplet evaporation. This time period corresponds to the horizontal
500 segment of the $\tilde{N}-\tilde{q}$ relationship in Fig. 5a. Fig. 6c shows the DSD at the stage when a
501 decrease in LWC is accompanied by a decrease in number droplet concentration. The
502 corresponding point in the $\tilde{N}-\tilde{q}$ diagram at this time instance is quite close to the point "F" at
503 which $\tilde{N}=0$ and $\tilde{q}=0$.

504 At $Da=50$, DSD are different at different $\tilde{x}$ during the entire period of mixing. While
505 DSD at $\tilde{x}>0.5$ are wide and droplet evaporation is accompanied by a shift of DSD maximum
506 to smaller droplet radii (this feature is typically attributed to homogeneous mixing), the DSD
507 maximum at $\tilde{x}<0.5$ (the initially cloud volume) shifts toward smaller radii only slightly until
508 $\tilde{t}=3.17$ (Fig. 6e). Further droplet evaporation either leads to a complete evaporation (at

509 $\tilde{x} \geq 0.5$) or shifts the DSDs to smaller droplet sizes (panel f). The maximum droplet
510 concentration takes place at $\tilde{x} = 0$. Fig. 6 shows that DSD shapes evolve substantially over
511 time, although the final state is characterized by complete droplet evaporation.
512
513 **5.2 Partial evaporation case**
514 **5.2.1 Evolution of the microphysical parameters at different values of Da and R**
515 Here we consider the process of mixing at $R > -1$, i.e. when not all the droplets evaporate
516 completely. **Figure 7** shows the horizontal profiles of a normalized supersaturation at different
517 Da and R. One can see that in all cases, the final state occurs when the equilibrium
518 supersaturation $\tilde{S} = 0$ (RH=100%). However, this final value is reached quite differently
519 depending on Da. At $Da = 1$, rapid mixing leads to formation of spatially homogeneous
520 humidity and supersaturation during a time period of a fraction of τ_{pr}. Then, supersaturation
521 within the mixing volume grows by evaporation of droplets, which are uniformly distributed
522 over the entire mixing volume. This process of homogeneous mixing was analyzed in detail in
523 Pt. 2.
524 At $Da = 500$, changes in supersaturation take place largely within the initially droplet-free
525 volume. RH in the initially cloud volume undergoes only small changes. This process agrees
526 well with the classical concept of extremely inhomogeneous mixing. However, a strong
527 gradient of supersaturation remains within the initially drop-free volume for a long time (tens
528 of τ_{pr}). At $Da = 50$, the situation is intermediate. Mixing is intensive enough to decrease RH
529 in the initially cloud volume, but spatially uniform RH is established within about 5-10 τ_{pr},
530 increasing with an increase in $|R|$. After this time instance, mixing takes place according to the
531 homogeneous scenario.
532 **Figure 8** shows the horizontal profiles of normalized LWC at different Da and R. At the
533 same R, the final equilibrium values of LWC are identical, as follows from Eq. (30); LWC

534 decreases with an increase in $|R|$. At any Da, the decrease in the LWC in the cloud volume is
535 caused largely by diffusion of droplets from the cloud volume into the initially droplet-free
536 volume .

537 At $Da = 500$, evaporation in the cloud volume is small because $\tilde{S}$ in these volumes is high
538 in cloud volumes during mixing (Fig. 7). At $Da = 1$, the process of spatial homogenization
539 takes place during fractions of τ_{pr}, i.e. $T_{mix} < 1$. Then, during a relatively lengthy period of
540 $10\tau_{pr}$, evaporation decreases LWC over the entire mixing volume, which is characteristic of
541 homogeneous mixing. At $Da = 50$, spatial homogenization takes place during about $T_{mix} \approx 15$.
542 This is a slightly shorter time than it takes to establish the final equilibrium stage T_{tot}. Different
543 Da's cases reach equilibrium at different times. The process of reaching a final uniform LWC
544 lasts for $100\tau_{pr}$ at $Da = 500$ and for about τ_{pr} at $Da = 1$.

545 **Figure 9** shows the profiles of the normalized droplet concentrations at different Da and
546 R. In contrast to LWC, the final concentration depends both on Da and R. Hence, profiles at
547 different *Da* can have different shapes at the same value of R. At $R = -0.1$ (which corresponds
548 to high RH in the initially dry volume) none of the droplets evaporate, so the final normalized
549 droplet concentration is equal to $\tilde{N} = 1/2$. This means that all the droplets in the initially cloud
550 volume are now uniformly distributed between both mixing volumes. At larger $|R|$, i.e., at
551 lower RH in an initially droplet-free volume, some droplets evaporate completely. The final
552 concentration decreases with an increase in Da.

553 The physical interpretation of this dependence is clear. At low Da, fast mixing leads to
554 formation of a uniform RH throughout the entire mixing volume, and this affects all the
555 droplets. At high Da, RH in the initially droplet -free volume remains low for a long time,
556 and droplets that penetrate can evaporate. Therefore, the fraction of completely evaporated
557 droplets increases with Da: at $R = -0.1$ there are no completely evaporated droplets at any *Da*.

558 At $R=-0.3$ a decrease in the droplet concentration takes place only at $Da=500$, and at
559 $R=-0.5$ the droplet concentration decreases already at $Da\geq 50$.

560 The comparative contributions of different factors in establishing the final states of mixing
561 are well seen in **Figure 10** presenting the relationships between normalized concentration and
562 normalized LWC at three values of $\tilde{x}$: 1/4 (centre of the cloudy volume), 1/2 and 3/4 (centre of
563 the initially dry volume) at $R=-0.5$ and different values of Da. Fig. 10 is analogous to Fig. 5,
564 but plotted for $R>-1$.

565 At $Da=1$ the mixing is very fast, which leads to a rapid decrease in LWC and in the
566 droplet concentration in the initially cloud volume and to an increase of these quantities in the
567 initially droplet-free volume. As a result of the rapid mixing and homogenization, all the curves
568 coincide at point "A" (left panel). After this time instance, spatial homogeneous evaporation
569 takes place. Since at $Da=1$ only partial, but not total, droplet evaporation occurs, the droplet
570 concentration remains unchanged even while LWC decreases. At $Da=50$ and $Da=500$, the
571 three curves coincide at the final point "F" only. At $Da=500$, the relationship between the
572 droplet concentration and the mass becomes more linear (blue curve). The linear dependence is
573 consistent with the concept of extremely inhomogeneous mixing (see Pt1). Considerations
574 regarding the closeness of the $\tilde{N}-\tilde{q}$ relationship to the line 1:1 as a measure of
575 inhomogeneity of mixing made at $R<-1$ are also valid for $R>-1$.

576

577 **5.2.2 Evolution of DSDs and the DSD parameters**

578 **Figure 11** presents examples of the DSD evolution at the center of the initially cloud
579 volume ($\tilde{x}=1/4$) (upper row) and of the initially droplet-free volume ($\tilde{x}=3/4$) at $R=-0.5$
580 and different values of Da. Several specific features of the DSD are notable. As a result of the
581 rapid mixing at $Da=1$ (left column), DSD become similar in both volumes already at
582 $t=0.317\tau_{pr}$ (black lines). Further evolution is similar in both volumes and is characterized by
583 broadening of the DSD and its shifting and of the DSD toward smaller droplet sizes. This shift

means a decrease in the mass at constant droplet concentration, which is typical of homogeneous mixing.

The initially monodisperse DSDs become polydisperse. The mechanism of the DSD broadening at $Da = 1$ is illustrated in **Figure 12**, showing the DSD at the earlier, inhomogeneous stage at different $\tilde{x}$. One can see that within very short periods when the spatial gradient of saturation deficit exists, droplets entering the initially droplet-free volume partially evaporate, reaching their minimal size at $\tilde{x} = 1$. In this way, a polydisperse DSD forms. As the mixing proceeds, DSD become spatially homogenized, as seen in the right panel of Fig. 12.

At $Da = 50$ and $Da = 500$, the DSD shapes substantially differ from those at $Da = 1$. There are two main differences: the peak of the distribution shifts only slightly (at $Da = 50$) or does not shift at all (at $Da = 500$). At the same time, the DSD develops a long tail of small droplets. Since the mixing rate at these values of Da is slow, droplets penetrating deeper into the initially dry volume remain there for long time and get smaller. As a result, at moderate and large Da, a polydisperse DSDs form with droplet sizes ranging from zero to 1. Formation of a long tail of small droplets in case of inhomogeneous mixing was simulated in direct numerical simulation (DNS) by Kumar et al. (2012), as well as by means of ‘‘the explicit-mixing parcel model’’ (EMPM) (Krueger et al., 1997; Su et al., 1998; Schlüter, 2006).

Figure 13 shows the spatial dependencies of the DSD dispersion (ratio of DSD r.m.s. width and the mean radius) at different time instances and different values of Da and R. One can see that the dispersion increases with an increase in Da and in $|R|$. This behavior can be accounted for by the fact that the DSD broadening toward smallest droplet size increases with the increase in Da and in $|R|$. The DSD dispersion increases with time and with an increase in $\tilde{x}$, i.e. further into the initially droplet free volume. At the same time, spatial homogenization takes place, so at the final state at $R = -0.5$ the DSD dispersion reaches 0.11 at $Da = 1$ and about 0.2 at $Da = 50$ and $Da = 500$.

610 Observed DSD dispersion in different clouds typically ranges from 0.1 to 0.4 (Khain et al.,
611 2000; Martin et al., 2004; Prabha et al., 2012) and can be caused the following factors: in-
612 cloud nucleation (e.g. Khain et al., 2000; Pinsky and Khain, 2002), spatial averaging along
613 aircraft traverses (Korolev, 1995) and non-symmetry in droplet nucleation/denucleation
614 (Korolev, 1995). As seen in Fig. 13, this dispersion may be also caused by mixing at cloud
615 edges at moderate and large Da. Hence, inhomogeneous mixing leads to DSD broadening.

616 The effective radius, r_{eff}, is an important DSD characteristic. According to the classical
617 concept, r_{eff} remains unchanged during extremely inhomogeneous mixing, whereas decreases
618 during homogeneous mixing. **Figure 14** shows spatial dependencies of r_{eff} at different time
619 instances and different values of Da and R. At $R = -0.1$ (high RH in the surrounding volume)
620 r_{eff} is similar for all values of Da. So, at high R (i.e., close to zero), the behaviour of r_{eff} does
621 not allow to distinguish between mixing types.

622 At a given R, the final r_{eff} increases with increasing Da. For instance, at $R = -0.5$, r_{eff} at
623 the final state differs from the initial r_{eff} value by less than 6% at $Da = 500$, while at $Da = 1$
624 r_{eff} decreases by 20%. At moderate and high Da, large gradients of r_{eff} exist during the
625 mixing process. However, the gradient is high only in the initially droplet-free volume where
626 r_{eff} decreases significantly due to the intense evaporation of droplets. Besides, r_{eff} growth very
627 rapidly in the initially droplet free volume, so at high Da during most of the mixing time r_{eff}
628 within the mixing volume becomes close to the initial r_{eff} value in the cloudy volume.

629

630 **5.3 Delimitation between mixing types**

631 Typically, the Da value is used as a criterion for delimitation between mixing types.
632 $Da = 1$ is usually used as a boundary value separating homogeneous and inhomogeneous
633 mixing. As shown in Section 4, mixing always starts as inhomogeneous. In the course of

634 mixing, the initial spatial gradients decrease and the air volumes either become identical or
635 remain different. In the former case, the second mixing stage is homogeneous. If
636 inhomogeneity persists until the equilibrium state is established, mixing remains
637 inhomogeneous during the entire period. Both mixing stages can be characterized by duration,
638 change in the droplet concentrations or LWCs, and other quantitative characteristics. These
639 characteristics are functions of two non-dimensional parameters R and Da, which can be
640 calculated and used for delimitation between mixing types. Since mixing between volumes
641 may turn from inhomogeneous into homogeneous before reaching the equilibrium state, it is
642 necessary to use some quantitative criteria to delimit mixing types. Below, delimitation is
643 performed for $R > -1$ which corresponds to partial evaporation of droplets by the end of
644 mixing.
645
646 **5.3.1. Characteristic time periods of mixing**
647 Three characteristic time periods of mixing are distinguished: a) mixing period T_{mix}, during
648 which spatial gradients are smoothening (may be also called the homogenization period) ; b)
649 period T_{ev} during which $S < 0$ and droplets evaporate until saturation is reached and c) the total
650 mixing period T_{tot} that lasts until the final equilibrium stage is reached. In our analysis, all the
651 three periods are assumed dimensionless quantities.
652 We use solution (28) for conservative function $\tilde{\Gamma}(\tilde{x},\tilde{t})$ to define quantitatively time period
653 T_{mix}. The deviation of the solution from its final value $\Delta\tilde{\Gamma} = \tilde{\Gamma}(\tilde{x},\tilde{t}) - \tilde{\Gamma}(\tilde{x},\infty)$ at $\tilde{t} \to \infty$ can be
654 approximately estimated using the first term of the series expansion as

655
$$\left|\Delta\tilde{\Gamma}\right|_{\max} \approx \left|(1-R)\frac{\sin(\pi/2)}{\pi/2}\exp\left(-\frac{\pi^2\tilde{t}}{Da}\right)\cos(\pi\tilde{x})\right|_{\max} = (1-R)\frac{2}{\pi}\exp\left(-\frac{\pi^2\tilde{t}}{Da}\right) \quad (37)$$

656 From Eq. (37) the estimation of T_{mix} can be written as

$$T_{mix} = -\frac{Da}{\pi^2}\ln\left[\frac{\pi}{2(1-R)}\left|\Delta\tilde{\Gamma}\right|_{\max}\right] \quad (38a)$$

Suppose the value of the maximum deviation is $\left|\Delta\tilde{\Gamma}\right|_{\max} = 0.02$. This is a small value compared to the initial leap of function $\tilde{\Gamma}$, which is equal to $1-R$. At $\left|\Delta\tilde{\Gamma}\right|_{\max} = 0.02$ the duration of the non-homogeneous stage is evaluated as

$$T_{mix} = -\frac{Da}{\pi^2}\ln\left[\frac{0.01\pi}{1-R}\right] \quad (38b)$$

Several studies evaluate the evaporation time for droplets of a particular size using the equation for diffusion growth (e.g. Lehmann et al., 2009). In our study, the evaporation time duration T_{ev} is defined as the period during which the maximum deviation of supersaturation from zero exceeds the small value chosen as $\left|\Delta\tilde{S}\right|_{\max} = 0.02$:

$$\left|\tilde{S}(\tilde{x}, T_{ev})\right| \le \left|\Delta\tilde{S}\right|_{\max} = 0.02 \quad (39)$$

Although criterion (39) is rather subjective, it has an advantage over the criterion used by Lehmann et al. (2009), as Eq. (32) characterizes evaporation of the droplet population taking into account the simultaneous increase in supersaturation, but not of individual droplets of particular size at constant S as in Lehmann et al. (2009).

At the end of the mixing, both the thermodynamic equilibrium and the diffusion equilibrium are reached. Accordingly, the total time of mixing T_{tot} is evaluated as the maximum of the two time periods needed to achieve equilibrium $T_{tot} = \max\{T_{mix}, T_{ev}\}$. All the three characteristic time periods are normalized on the phase relaxation time, and, therefore, depend on the two non-dimensional parameters R and Da. The contours of the characteristic time durations T_{mix}, T_{ev} and T_{tot} in the $Da-R$ diagrams are shown in **Figure 15.**

680 As follows from Eq. (38b), T_{mix} is proportional to Da. The dependence of T_{mix} on R is not
681 very strong, so T_{mix} slightly decreases with increasing R. This can be attributed to the fact that
682 the lower R, the smaller the initial inhomogeneity of function $\tilde{\Gamma}$ and the shorter the time to
683 align this inhomogeneity is. At small Da (high rate of homogenization of the volume), T_{ev}
684 depends largely on R. At large Da, T_{ev} depends substantially on Da, since the evaporation
685 rate depends on the number of droplets that diffuse to drier parts of the mixing volume. A
686 comparison of Fig. 15c with Figs. 15a and 15b shows that at small Da, time T_{tot} is determined
687 by T_{ev}, while at large Da, T_{tot} is determined by T_{mix}.
688
689 **5.3.2. Determination of boundaries between the mixing types on the $R-Da$ plane**
690 Several criteria can be proposed for delimitation between mixing types. We consider these
691 criteria for $R>-1$. As discussed above, mixing always starts as inhomogeneous and late either
692 become homogeneous or remains inhomogeneous till the final equilibrium state is established.
693 At small Da, the homogenization takes place during $T_{mix}<T_{tot}$. The value of time fraction λ_1 of
694 the inhomogeneous stage can serve as a criterion for definition of homogeneous mixing. This
695 formula for the fraction can be written as
696 $$\lambda_1=\frac{T_{mix}}{T_{tot}} \qquad (40)$$
697 The case $\lambda_1\le 0.5$, most time the mixing takes place according the homogeneous scenario and
698 such regime is reasonable to regard as homogeneous mixing. If $\lambda_1(R,Da)$ changes within the
699 range of $0.5<\lambda_1\le 1$, mixing appears to be intermediate. The criterion (40) depends on the non-
700 dimensional parameters R and Da. **Figure 16a** shows the boundaries separating mixing types _
701 on the $Da-R$ plane. These boundaries separate all plane into several zones. At very small R,
702 the duration of the phase transition is negligibly small. According to criterion (40), in this case
703 mixing should be considered inhomogeneous, irrespective of the Da value.

Another criterion of delimitation between mixing types can be determined from a comparison of LWC variation rates due to different mechanisms. The mean normalized LWC (which is equal to the mean normalized liquid water mixing ratio) can be written as integral $\langle \tilde{q}(\tilde{t}) \rangle = \int_0^1 \tilde{q}(\tilde{x},\tilde{t}) d\tilde{x}$. The initial mean LWC is equal to $\langle \tilde{q}(t=0) \rangle = \frac{1}{2}$. The final equilibrium LWC is equal to $\langle \tilde{q}(t=\infty) \rangle = \frac{1}{2}(1+R)$ (Eq. (30)). The total amount of liquid water that evaporates in the course of mixing can be quantified by the difference between these two values $\langle \tilde{q}(t=0) \rangle - \langle \tilde{q}(t=\infty) \rangle = -\frac{1}{2}R$. The amount of liquid water evaporated in the course of the first inhomogeneous mixing stage is calculated by the equation $\langle \tilde{q}(t=0) \rangle - \langle \tilde{q}(T_{mix}) \rangle = \frac{1}{2} - \langle \tilde{q}(T_{mix}) \rangle$. Hence, parameter λ_2 which is a ratio of

$$\lambda_2 = \frac{\langle \tilde{q}(t=0) \rangle - \langle \tilde{q}(T_{mix}) \rangle}{\langle \tilde{q}(t=0) \rangle - \langle \tilde{q}(t=\infty) \rangle} = \frac{2\langle \tilde{q}(T_{mix}) \rangle - 1}{R} \qquad (41)$$

can serve as another possible criterion for delimitation between mixing types. This ratio characterizes the fraction of liquid water that evaporates at the initial inhomogeneous stage. Condition $\lambda_2 < 0.5$ in this case corresponds to homogeneous mixing, while condition $0.5 \le \lambda_2 < 1$ corresponds to intermediate mixing. We regard the case $\lambda_2 = 1$ as inhomogeneous mixing. Certainly, criterion λ_2 depends on the non-dimensional parameters R and Da. Fig. 16b illustrates delimitation between mixing types on the $Da - R$ plane according to criterion λ_2.

Comparison of Figs. 16a and 16b shows that both criteria lead to nearly similar separation of the $Da - R$ plane into three zones corresponding to homogeneous, intermediate and inhomogeneous mixing. At the same time, the boundaries separating these zones are different depending on the delimitation criterion used. Nevertheless, it can be concluded that mixing can

726 be considered homogeneous at Da below 4-10 and $R < -0.1$ and inhomogeneous at Da
727 exceeding several tens.

728 Terms "inhomogeneous mixing" (Burner and Brenguier, 2007) and "extremely
729 inhomogeneous mixing" (Lehmann et al., 2009; Gerber et al., 2008; Pt1) are used to denote the
730 mixing regime when the relationship between the normalized values $\tilde{N}$ and $\tilde{q}$ is represented
731 by a straight 1:1 line, which is equivalent to the constant mean volume radius (in some studies,
732 the effective radius is used instead of the mean volume radius. According to the definition used
733 in the present study, extremely inhomogeneous mixing is the limiting case of inhomogeneous
734 mixing when $Da \to \infty$. Despite the fact that the extremely inhomogeneous mixing is only a an
735 idealization our approach allows to determine to what extent mixing can be considered to be
736 close to this limiting case. The measure of inhomogenity of mixing is the closeness of the
737 $\tilde{N} - \tilde{q}$ relationship to the 1:1 straight line (see discussion above related to Figs. 5 and 10).

738 **Figure 17a** shows r.m.s. distance between the $\tilde{N} - \tilde{q}$ relationship and the 1:1 straight line,
739 depending on Da and R. These dependences were calculated using the set of points $\tilde{N}_i, \tilde{q}_i$
740 uniformly distributed over spatial interval $0 \div 1$ and time interval $0 \div T_{tot}$. The equation for
741 estimation is $\delta = \sqrt{\frac{1}{2M}\sum_{i=1}^{M}\left(\tilde{N}_i - \tilde{q}_i\right)^2}$, where M is the total number of points. This distance
742 corresponds to r.m.s. deviation of the normalized mean volume radius from 1. The dependences
743 of the last deviation on Da and R and estimated as $\delta/3$ are shown in Fig. 17b. This estimation
744 is based on the fact that the total mass of droplets is proportional to the cube of the mean
745 volume radius. As expected, the distance decreases with increasing in Da. At large R, all the
746 curves coincide indicating a degenerative case when type of mixing becomes indistinguishable.

747 We choose the value $\delta/3$ equal to 0.02 to determine the boundary of the extremely
748 inhomogeneous mixing zone. The value of 0.02 corresponds to droplet radii deviation of a few
749 tenths of a micron, which is so low that in in-situ measurements this case would always be
750 attributed to extremely inhomogeneous mixing. In Fig.16 this boundary is marked by broken

751 line. The boundary shows that the mixing at Da exceeding several hundred can be attributed
752 to the extremely inhomogeneous. Between the boundary separating inhomogeneous mixing
753 from the intermediate one and the boundary separated inhomogeneous mixing from extremely
754 inhomogeneous there exists a wide zone of inhomogeneous mixing where the mean volume (or
755 the effective) radius may drop by 10% and more (Fig. 14), and where the DSD dispersion is
756 substantial and the tail of small droplets is long enough (Fig. 11). Mixing diagrams currently
757 used for analysis of observed data ($N-q$ dependences in the final equilibrium state of mixing)
758 do not contain this zone which, therefore, has remained unrecognized and uninvestigated.
759

760 **6. Summary and conclusions**

761 In this study, inhomogeneous turbulent mixing is investigated using a simple a 1D model of
762 mixing between a saturated cloud volume and an undersaturated droplet-free volume. The
763 mixing is simulated by solving a diffusion-evaporation equation written in the non-dimensional
764 form. For simplicity, the initial volumes of cloudy and droplet-free air were assumed to be
765 equal, and the initial DSD in the cloudy volume was assumed monodisperse.

766 Analysis of the diffusion-evaporation equation shows that the time-dependent process of
767 mixing and the final equilibrium state depend on two non-dimensional parameters. The first
768 parameter R, referred in this paper as potential evaporation parameter (PEP) is proportional to
769 the ratio between the saturation deficit in the initially droplet-free volume and the initial liquid
770 water content in the cloudy volume. At $R<-1$, the final state is characterized by complete
771 droplet evaporation and a spatially homogeneous saturation deficit, which indicates dissipation
772 of the cloudy volume. At $R>-1$, the final state is characterized by existence of droplets and
773 zero saturation deficit (RH=100%). In this case, the cloud volume expands after mixing with the
774 entrained air. At small values of $|R|$ (e.g., when RH in the entrained volume is close to 100%),
775 the effect of droplet evaporation on microphysics is small, and, formally, this kind of mixing
776 should be regarded as extremely inhomogeneous. Strictly speaking, this is a degenerate case,

777 when homogeneous and inhomogeneous mixing cannot be distinguished (see also Pt. 1). At
778 $R = 0$, the droplet population turns into a passive admixture and its turbulent diffusion will be
779 the same as different thermodynamic parameters.

780 The second parameter is the *Damkölher* number (Da) which is the ratio between the
781 characteristic mixing time and the phase relaxation time. This parameter compares the rates of
782 spatial diffusion and evaporation. Parameter Da (Eq. (23)) is logically appears in the non-
783 dimensional form of the diffusion-evaporation equation showing that Da is the ratio of the
784 mixing time defined as $\tau_{mix} = \frac{L^2}{K}$, to the initial drop relaxation time. The expression for this non-
785 dimensional parameter clearly shows that since we consider an ensemble of evaporating droplets,
786 the drop relaxation time evaluated just before the mixing is the characteristic time scale of
787 inhomogeneous mixing process. In several studies (e.g., Baker and Latham, 1979; Burnet and
788 Brenguier, 2007; Andejchuk et al., 2009) a question was raised as to which time scale should be
789 used in formulation of the *Damkölher* number: the time of an individual droplet evaporation at
790 constant saturation deficit, or the phase relaxation time. This study, as well Pt. 2 show that the
791 phase relaxation time is the answer. The mixing time is introduced via the turbulent diffusion
792 coefficient which is a natural measure characterizing the diffusion rate and, in particular,
793 determines the propagation rate of the fronts in the fields of droplet concentration and other
794 microphysical parameters. The turbulent diffusion coefficient is widely used to describe mixing
795 in cloud models at resolved scales.

796 The analysis was performed within a wide range of Da (from 1 to 500) and of R (from -
797 1.5 to -0.1). The final LWC and the humidity in the mixing volume are determined by the mass
798 conservation and do not depend on Da (see also Pt. 1 and Pt. 2). At the same time, the droplet
799 concentration, as well as the shape of DSD and their parameters strongly depend on Da.

800 It is shown that the mixing of air volumes with initially different thermodynamical and
801 microphysical parameters consists of two stages characterized by two time periods: the time

802 during which microphysical characteristics become uniform over the total mixing volume T_{mix},
803 and the time during which zero saturation deficit is reached (at $R > -1$), T_{ev}. At $\tilde{t} < T_{mix}$, the
804 spatial gradients of the microphysical values remain and the mixing regime can be regarded as
805 inhomogeneous. At $\tilde{t} > T_{mix}$, droplet evaporation, if it occurs at all, takes place within a
806 spatially homogeneous medium, so all the droplets in the mixing volume experience equal
807 saturation deficit. This regime can be regarded as homogeneous. It is shown, therefore, that at
808 small Da mixing between two volumes that starts as inhomogeneous can become
809 homogeneous towards the end of mixing.

810 This finding allows to delimit between mixing types. We presented two quantitative criteria
811 on the $Da - R$ plane that allow to delimit three mixing regimes: homogeneous, intermediate
812 and inhomogeneous. These criteria are based on comparison of the characteristic duration
813 mixing and the evaporation rates. According to the criteria, at Da below about 5, mixing can
814 be regarded as homogeneous, i.e. the main microphysical changes take place during the
815 homogeneous stage. At $5 < Da < 30 \div 50$, the changes in the microphysical parameters are
816 more significant at the inhomogeneous stage than at the homogeneous stage. In this case, the
817 mixing can be regarded as intermediate. Finally, at Da exceeding several tens, the spatial
818 microphysical gradients remain until the final equilibrium stage is reached. In this case, the
819 mixing can be regarded as inhomogeneous. At Da exceeding a few hundred the deviations
820 from predictions based of the classical concept of extremely inhomogeneous become relatively
821 small, which justifies attribute regarding this mixing as extremely inhomogeneous.

822 On the whole, the results of the present study are in line with the classic concepts defining
823 homogeneous and inhomogeneous mixing types. However, several important points emerge
824 from our work show serious limitations of classical concepts. A comparison of the classical
825 concepts and the present study is presented in **Table 2**. Analysis of Tab. 2 shows the following.

826 a) In contrast to many studies that analyze only the hypothetical final (equilibrium) state of
827 mixing (Barnet and Brenguier, 2007; Gerber et al., 2008; Morrison and Grabowski, 2008; Hill

et al., 2009), we consider the entire time-dependent processes of mixing and evaporation. At moderate and high Da, the mixing can last several minutes. In in-situ observations, we see mostly non-equilibrium stages which may account for a rather wide scattering of mixing diagrams even at the same values of Da (e.g., Lehmann et al., 2009).

Note that time dependent mixing was also considered in several studies (e.g. Baker et al., 1980; Baker and Latham, 1982; Jeffery and Reisner, 2006; Krueger et al., 1997; Kumar et al., 2012) using different approaches and numerical models. These studies, however, do not contain analysis on non-dimensional diffusion-evaporation equation.

b) It is also shown in the study that the slopes of the $\tilde{N} - \tilde{q}$ relationship (between the normalized droplet concentration and LWC) tends to the 1:1 line with increasing Da. The closeness can be considered as a measure of extremely inhomogeneous mixing in terms of the classical concept (see Pt. 1). It has been found that the slope of the $\tilde{N} - \tilde{q}$ relationship depends on the LWC and, accordingly, on time. At large LWC, $\tilde{q}$ changes with time faster than $\tilde{N}$, while at low LWC the concentration changes faster. Although mixing types are usually separated into homogeneous and extremely inhomogeneous, we have shown that there are wide ranges of Da and R at which mixing should be considered intermediate or inhomogeneous, but not extremely inhomogeneous. Within these ranges the effective radius can change by more than 10-15%. Standard mixing diagrams do not include this range that, to our knowledge, has never been investigated despite the fact that multiple in-situ measurements indicate its existence .

c) Many studies assume the existence of pure homogeneous mixing during which the initially monodisperse DSD remains monodisperse. Our study shows that at the very beginning, mixing is always inhomogeneous. This inhomogeneous stage leads to formation of a polydisperse DSD that broadens in the course of droplet evaporation. Hence, even at $Da = 1$ the initially monodisperse spectrum becomes polydisperse.

d) It is shown that at small Da, mixing includes both inhomogeneous and homogeneous stages, which means that type of mixing can change during the mixing process.

e) The classical concept assumes that the effective radius always decreases during homogeneous mixing. Assuming an initially monodisperse DSD, we have found this conclusion largely valid, with the exception small R. At the same time, it was shown in Pt. 2 that during homogeneous mixing, the effective radius can decrease, remain constant or increase depending of the initial DSD shape. Thus, a decrease in the effective radius during mixing cannot always be considered an indication of homogeneous mixing. Similarly, the invariability the effective radius during mixing in the process cannot always be considered an indication of extremely inhomogeneous mixing.

f) It is generally assumed that during homogeneous mixing droplet concentration remains unchanged. In the present study, as well as in Pt. 2, it is shown that since mixing leads to a polydisperse DSD, the smallest droplets may completely evaporate. At $R<-1$, the DSD becomes very wide and all the droplets, the smallest ones first, evaporate.

g) It is generally assumed that inhomogeneous mixing does not alter DSD shape, but only decreases droplet concentration. The present study showed that inhomogeneous mixing significantly changes the DSD shape. DSD were found to be quite different in different regions of mixing volumes. The main feature is the DSD broadening toward small droplet size, so the relative dispersion grows up to 0.2-0.3. These values are quite close to those observed in atmospheric clouds (Khain et al., 2000). Elongated tails of small droplets during mixing were simulated by Schlüter (2006) who described turbulent diffusion following to Kruger et al., (1997) and Su et al., (1998) as well as by Kumar et al. (2012) using DNS. We see that formation of a polydisperse DSD is a natural result of inhomogeneous mixing and, therefore, inhomogeneous mixing is an important mechanism of DSD broadening. A significant impact of mixing on DSD shape was found identified in multiple studies, beginning with Warner (1973).

879 h) The effective radius has been assumed to remain constant during extremely
880 inhomogeneous mixing. Our results indicate that, indeed, at the final equilibrium stage at
881 comparatively high RH the effective radius is close to that in the initially cloudy volume
882 (especially at high Da). At the same time, we found that the effective radius varies in size and
883 is smaller in the initially droplet-free volumes.

884 The results obtained in parts Pt1 and Pt 2, and especially in the current study (Pt 3)
885 dedicated to analysis of turbulent mixing mechanisms in clouds determine the directions for
886 future work. Since the widely used mixing diagrams show only a hypothetical equilibrium
887 state, but not the instantaneous state of mixing that likely correspond to transition periods, the
888 efficiency of the standard mixing diagrams is questionable. Moreover, the standard diagrams
889 miss a very important mixing regime, namely, inhomogeneous mixing that occurs between two
890 limiting cases of homogeneous and extremely inhomogeneous mixing (Fig. 16).

891 We believe that the results obtained will help to improve understanding and interpretation
892 of mixing process both in in-situ measurements and modeling. The approach allows to
893 investigate the relationship between the main microphysical parameters typical of
894 inhomogeneous mixing, that differ from those in the limiting cases of extremely
895 inhomoheneous mixing. In addition, utilization of polydisperse DSD when solving diffusion-
896 evaporation equation allows to investigate the role of the initial DSD shape in mixing. In-situ
897 measurements (e.g., Burnet and Brenguier, 2007; Gerber et al., 2008; Lehmann et al., 2009)
898 and numerical models (Magaritz-Ronen et al., 2016) show a wide scattering of data on the
899 scattering diagrams. We expect location of various points on the diagrams (e.g. r_v^3 vs. dilution
900 rates) depends on the shape of the initial DSDs and characterizes the stage of mixing. The
901 method applied in the study allows investigation of evolution of DSD moments over space and
902 time .

903 Recently, there has been vigorous discussions concerning the possible existence of high
904 humidity layer near cloud edges that might affect mixing of cloud with its surrounding (Gerber

et al., 2008; Lehmann et al., 2009). In our opinion, this layer does exist and forms as a result of turbulent mixing of cloud with surrounding dry air, accompanied by complete droplet evaporation. The approach developed in the present paper allows to analyze formation of such humid layers.

We believe that the results obtained in this study will foster the development of physically grounded parameterization of mixing in cloud models.

Acknowledgements

This research was supported by the Israel Science Foundation (grant 1393/14), the Office of Science (BER), the US Department of Energy Award DE-SC0006788 and the Binational US-Israel Science Foundation (grant 2010446). Dr. Korolev's participation was supported by Environment Canada.

Appendix. List of symbols

Table A here

930

931 **References**

932 Andrejczuk M., W. Grabowski, S. P. Malinovski, P. K. Smolarkiewicz, 2009: Numerical
933 Simulation of Cloud–Clear Air Interfacial Mixing: Homogeneous versus Inhomogeneous
934 Mixing. *J. Atmos. Sci*., **66**, 2993-2500.

935 Baker, M., and J. Latham: The evolution of droplet spectra and the rate of production of
936 embryonic raindrops in small cumulus clouds. *J. Atmos. Sci.*, **36,** 1612–1615, 1979.

937 Baker, M., R. G. Corbin, and J. Latham: The influence of entrainment on the evolution of
938 cloud drop spectra: I. A model of inhomogeneous mixing. *Quart. J. Roy. Meteor. Soc.*, **106,** 581–
939 598, 1980.

940 Baker M. B. and J. Latham: A diffusive model of the turbulent mixing of dry and cloudy
941 air *Quart. J. R. Met.* Soc., **108**, 871-898, 1982

942 Burnet, F., and J.-L Brenguier, Observational study of the entrainment-mixing process in
943 warm convective cloud, *J. Atmos. Sci*., 64, 1995–2011, 2007.

944 Blyth, A. M., Choularton, T. W., Fullarton, G., Latham, J., Mill, C. S., Smith, M. H., and
945 Stromberg, I. M.: The Influence of entrainment on the evolution of cloud droplet spectra. 2.
946 Field experiments 5 at Great Dun Fell, *Q. J. Roy. Meteor. Soc*., **106**, 821–840, 1980.

947 Boffetta G. and I. M. Sokolov: relative dispersion in fully developed turbulence: The
948 Richardson's law and intermittency correction. Phys. Rev. Let**., 88**, 094501, 2002.

949 Denvich B. J., P. Bartello, J-L. Brenguier, L.R. Collins, W.W. Grabowski, R.H.A.
950 Ijzermans, S.P. Malinovski, M.W. Reeks, J.C. Vassilicos, L-P. Wang, and Z. Warhaft: Droplet
951 growth in warm turbulent clouds. *Q. J. Roy. Meteorol. Soc.*, **138**, 1401-1429, 2012

952 Gerber H, Frick G, Jensen J.B, and Hudson J.G.: Entrainment, mixing, and microphysics in
953 trade-wind cumulus. *J. Meteorol. Soc. Jpn.*, **86A**. 87-106, 2008.

954 Hill, A. A., G. Feingold, and H. Jiang: The Influence of Entrainment and Mixing
955 Assumption on Aerosol–Cloud Interactions in Marine Stratocumulus. *J. Atmos. Sci.*, **66**, 1450–
956 1464, 2009.

957 Jeffery, C.A., and J.M. Reisner: A study of cloud mixing and evolution using PDF methods.
958 Part I: Cloud front propagation and evaporation. *J. Atmos. Sci*., **63**, 2848-2864, 2006.

959 Khain, A. P**.,** M. Ovchinnikov, M. Pinsky, A. Pokrovsky, and H. Krugliak: Notes on the
960 state-of-the-art numerical modeling of cloud microphysics. *Atmos. Res.* **55**, 159-224, 2000.

961 Korolev, A.V.: The influence of suresaturation fluctuations on droplet size spectra
962 formation. *J. Atmos. Sci.*, **52**, 3620-3634, 1995.

963 Korolev A., and I. Mazin: Supersaturation of water vapor in clouds, *J. Atmos. Sci*., **60**,
964 2957-2974, 2003.

965 Korolev A., A. Khain, M. Pinsky, and J. French: Theoretical study of mixing in liquid
966 clouds. Part 1: classical concept. *Atmos. Chem. Phys.* , 2015 (submitted)

967 Kovetz, A., and B. Olund: The effect of coalescence and condensation on rain formation in
968 a cloud of finite vertical extent. *J. Atmos. Sci.,* **26,** 1060–1065, 1969.

969 Krueger S., C.-W. Su and P. McMurtry: Modeling entrainment and finescale mixing in
970 cumulus clouds. *J. Atmos. Sci*., **54**, 2697-2712, 1997

971 Kumar B., F. Janetzko, J. Schumacher, and R. A. Shaw: Extremely responses of a coupled
972 scalar-particle system during turbulent mixing. *New J. of Phys.* **14**, 115020 , 2012

973 Latham, J. and Reed, R. L.: Laboratory studies of effects of mixing on evolution of cloud
974 droplet spectra, *Q. J. Roy. Meteor. Soc*., **103**, 297–306, 1977.

975 Lehmann, K.., H. Siebert, and R. A. Shaw: Homogeneous and inhomogeneous mixing in
976 cumulus clouds: Dependence on local turbulence structure. *J. Atmos. Sci*., **66**, 3641-3659, 2009.

977 Magaritz-Ronen L., A. Khain and M. Pinsky, 2016: About the Horizontal Variability of
978 Effective Radius in Stratocumulus Clouds. *J. Geophys. Res*. (in revision)

979 Martin G.M., D. W. Johnson and A. Spice: The measurements and parameterization of
980 effective radius of droplets in warm stratocumulus clouds. *J. Atmos. Sci.*, **51**, 1823-1842, 1994.
981 Monin, A.S. and Yaglom, A.M.: "Statistical Fluid Mechanics: Mechanics of Turbulence",
982 vol. **2**, MIT Press. 1975
983 Morrison, H., and W. W. Grabowski: Modeling supersaturation and subgrid-scale mixing
984 with two-moment bulk warm microphysics. *J. Atmos. Sci.*, **65,** 792–812, 2008.
985 Pinsky, M. and A. P. Khain: Effects of in-cloud nucleation and turbulence on droplet
986 spectrum formation in cumulus clouds. *Quart. J. Roy. Meteorol. Soc*., 128, 1–33, 2002.
987 Pinsky M**.**, I. P. Mazin, A. Korolev, and A. Khain: Supersaturation and diffusional droplet
988 growth in liquid clouds. *J. Atmos. Sci.*, **70**, 2778-2793, 2013.
989 Pinsky M., I. P. Mazin, A. Korolev and A. Khain: Supersaturation and diffusional droplet
990 growth in liquid clouds: Polydisperse spectra. *J. Geophys. Res., Atmospheres*, **119**, 12,872–
991 12,887, 2014.
992 Pinsky, M., Khain, A., Korolev, A., and Magaritz-Ronen, L.: Theoretical study of mixing in
993 liquid clouds. Part 2: Homogeneous mixing. *Atmos. Chem. Phys.*, , 2016 (submitted)
994 Polyanin A. D. and V. F. Zaitsev: Handbook of nonlinear partial differential equations.
995 Chapman & Hall/CRC, 809 pp. , 2004
996 Prabha V. T., S. Patade, G. Pandithurai**,** A. Khain, D. Axisa, P. Pradeep Kumar, R. S.
997 Maheshkumar, J. R. Kulkarni, and B. N. Goswami: Spectral width of premonsoon and
998 monsoon clouds over Indo-Gangetic valley during CAIPEEX, *J. Geop. Res.* **117**, D20205,
999 doi:10.1029/2011JD016837 ', 2012
1000 Pruppacher, H.R., Klett, J.D.. Microphysics of Clouds and Precipitation. 2nd edn. Oxford
1001 Press, 914 p. , 1997
1002 Rogers R. R. and Yau M. K: A Short Course in Cloud Physics, Pergamon press. 293pp. ,
1003 1989

Schlüter M. H.: The effects of entrainment and mixing process on the droplet size distribution in cumuli. A thesis submitted to the faculty of The University of Utah in partial fulfillment of the requirements for the degree of Master of Science, Department of Meteorology, The University of Utah, 92 pp., 2006

Su C.-W., S.K. Krueger, P.A. McMurtry and P.H. Austin: Linear eddy modeling of droplet spectral evolution during entrainment and mixing in cumulus clouds. *Atmos. Res*., **47-48**, 41-58, 1998.

Telford, J.W., and S. K. Chai: A new aspect of condensation theory. *Pageoph*, **118**, 720-742 , 1980

Warner, J.: The microstructure of cumulus cloud. Pt. I, General features of the droplet spectrum, *J. Atmos. Sci***., 26,** 1049-1059, 1969.

Warner, J.. The microstructure of cumulus cloud: Part 4: The effect on the droplet spectrum of mixing between cloud and environment. *J. Atmos. Sci*. **30**, 256–261, 1973.

Table 1. Main parameters of the problem and their non-dimensional forms*

Quantity	Symbol	Non-dimensional form	Range of normalized values
Time	t	$\tilde{t} = \frac{t}{\tau_0}$	$[0...\infty]$
Distance	x	$\tilde{x} = \frac{x}{L}$	$[0...1]$
Square of drop radius	σ	$\tilde{\sigma} = \frac{\sigma}{r_0^2}$	$[0...1]$
Droplet concentration	N	$\tilde{N} = \frac{N}{N_1}$	$[0...1]$
Liquid water mixing ratio	q	$\tilde{q} = \frac{q}{q_1}$	$[0...1]$
Distribution of square of drop radius	$g(\sigma)$	$\tilde{g}(\tilde{\sigma}) = \frac{r_0^2}{N_1} g(\sigma)$	
Conservative function	Γ	$\tilde{\Gamma} = \frac{\Gamma}{A_2 q_1}$	$[-\infty...1]$
Supersaturation	S	$\tilde{S} = \frac{S}{A_2 q_1}$	$[-\infty...0]$
Relaxation time	τ_{pr}	$\tilde{\tau}_{pr} = \frac{\tau_{pr}}{\tau_0}$	$[1...\infty]$
Damkölher number	Da	$Da = \frac{\tau_{mix}}{\tau_0} = \frac{L^2}{K\tau_0}$	$[0...\infty]$
Potential evaporation parameter (PEP)	R	$R = \frac{S_2}{A_2 q_1}$	$[-\infty...0]$

*All normalized values depend on the initially given values of L, N_1, r_0, A_2, S_2 and K

1036

1037 **Table 2.** Comparison of analysis based on the classic concepts of mixing and the results of
1038 the present study

1039

Classical concept	The present study
Only the final equilibrium state is typically analyzed; results of in-situ observations are interpreted assuming the equilibrium state.	The mixing period can last several minutes and more. The microphysical structure of the mixing volumes during this period can differ substantially from that at the final state
Types of mixing are separated into homogeneous and extremely inhomogeneous.	There are the wide ranges of Da and R values, at which mixing can be regarded as intermediate or inhomogeneous (but not extremely inhomogeneous).
Mixing can start as purely homogeneous	Any mixing starts with the inhomogeneous stage
Homogeneous mixing leads to a DSD shift to small droplet sizes	Homogeneous mixing does not always lead to the DSD shift to small droplet sizes (Pt. 2). The shift depends on the DSD shape.
Mixing can be analyzed within the framework of a monodisperse DSD	Mixing always leads to formation of polydisperse DSD
In the course of homogeneous mixing, droplet concentration remains constant	In the course of homogeneous mixing, droplet concentration does not always remain constant (Pt. 2)
Extremely inhomogeneous mixing does not change the DSD shape	Inhomogeneous mixing (including extremely inhomogeneous) leads to broadening of the DSD towards small sizes

In the course of inhomogeneous mixing, the effective radius remains constant	The effective radius varies only slightly (5-20 %) in the initially cloud volume. The effective radius rapidly increases in the initially droplet-free volume, approaching the value of effective radius in the cloud volume. With increasing Da, the difference between the values of the effective radius in the initially cloud volume and that at the final state decreases in agreement with the classic concept.

1057 **Tab. A. List of symbols**

1058 ("nd" means non-dimensional)

Symbol	Description	Units
A_2	$\frac{1}{q_v}+\frac{L_w^2}{c_p R_v T^2}$, coefficient	nd
a_0, a_n	the Fourier series coefficients	nd
C	the Richardson's law constant	nd
c_p	specific heat capacity of moist air at constant pressure	J kg^{-1}K^{-1}
$\mathscr{D}$	coefficient of water vapour diffusion in the air	m^2 s^{-1}
Da	the *Damkölher* number	nd
e	water vapor pressure	N m^{-2}
e_S	saturation vapour pressure above a flat water surface	N m^{-2}
F	$F=\frac{\rho_w L_w^2}{k_a R_v T^2}+\frac{\rho_w R_v T}{e_S(T)\mathscr{D}}$, coefficient	m^{-2} s
$f(r)$	droplet size distribution	m^{-4}
$g(\sigma)$	distribution of square radius	m^{-5}
$\tilde{g}(\tilde{\sigma})$	normalized distribution of square radius	nd
k_a	coefficient of air heat conductivity	J m^{-1}s^{-1}K^{-1}
K	turbulent diffusion coefficient	m^{2}s^{-1}
L	characteristic spatial scale of mixing	m
L_w	latent heat for liquid water	J kg^{-1}
m_α	moment of DSD of order α	m^{-3}
N	droplet concentration	
$\tilde{N}$	normalized droplet concentration	nd
N_1	Initial droplet concentration in a cloud volume	m^{-3}
p	pressure of moist air	N m^{-2}
q	liquid water mixing ratio	kg/kg
q_1	Initial liquid water mixing ratio in a cloudy volume	kg/kg
q_v	water vapor mixing ratio	kg/kg
$\tilde{q}$	normalised liquid water mixing ratio equal to	nd

	normalized LWC	
r	droplet radius	m
r_0	initial droplet radius	m
r_0	mean droplet radius	m
r_v	mean volume radius	m
R	$\frac{S_2}{A_2 q_1}$, potential evaporation parameter (PEP)	nd
R_a	specific gas constant of moist air	J $kg^{-1}K^{-1}$
R_v	specific gas constant of water vapor	J $kg^{-1}K^{-1}$
S	$e/e_w - 1$, supersaruration over water	nd
$\tilde{S}$	normalized supersaturation	nd
S_2	Initial supersaturation in a dry volume	nd
$\tilde{S}_{\max}$	maximal normalized supersaturation	nd
T	temperature	K
T_{mix}	normalized duration of inhomogeneous stage	nd
T_{ev}	normalized duration of evaporation	nd
T_{tot}	normalized duration of mixing	nd
t	time	s
$\tilde{t}$	non-dimensional time	nd
x	distance	m
$\tilde{x}$	non-dimensional distance	nd
$\lambda_1,\ \lambda_2$	criteria of delimitation between the types of mixing	nd
ε	turbulent dissipation rate	m^2s^{-3}
$\Gamma(x,t)$	conservative function	nd
$\tilde{\Gamma}$	normalized conservative function	nd
ρ_a	air density	kg m^{-3}
ρ_w	density of liquid water	kg m^{-3}
σ	square of droplet radius	m^2
$\tilde{\sigma}$	normalized square of droplet radius	nd
τ_{pr}	phase relaxation time	s

$\tilde{\tau}_{pr}$	normalized phase relaxation time	nd
τ_{mix}	characteristic time of mixing	s
τ_0	Initial time scale	s

Figures

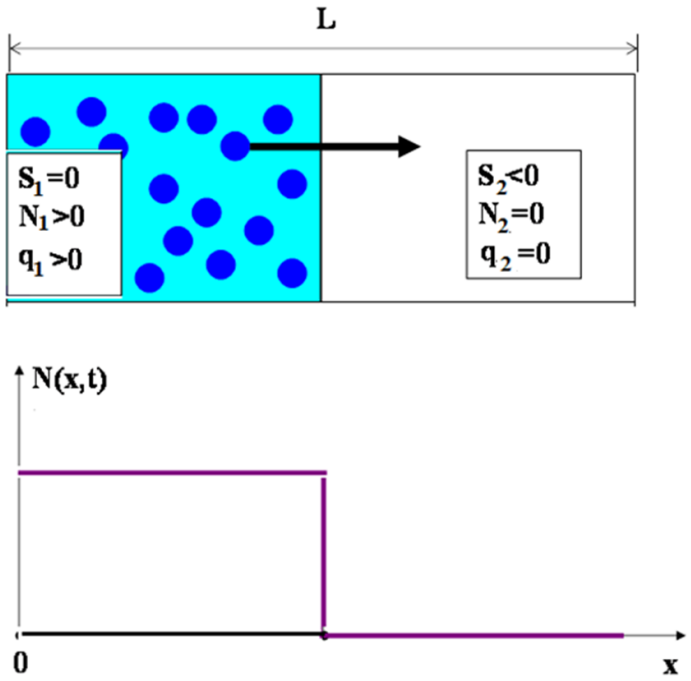

Fig.1. The schematic illustration of the 1D mixing problem considered in the study. The initial state at $t = 0$ is illustrated. The left volume of length $L / 2$ is a saturated cloudy volume; the right volume is a non-saturated air volume from the cloud environment.

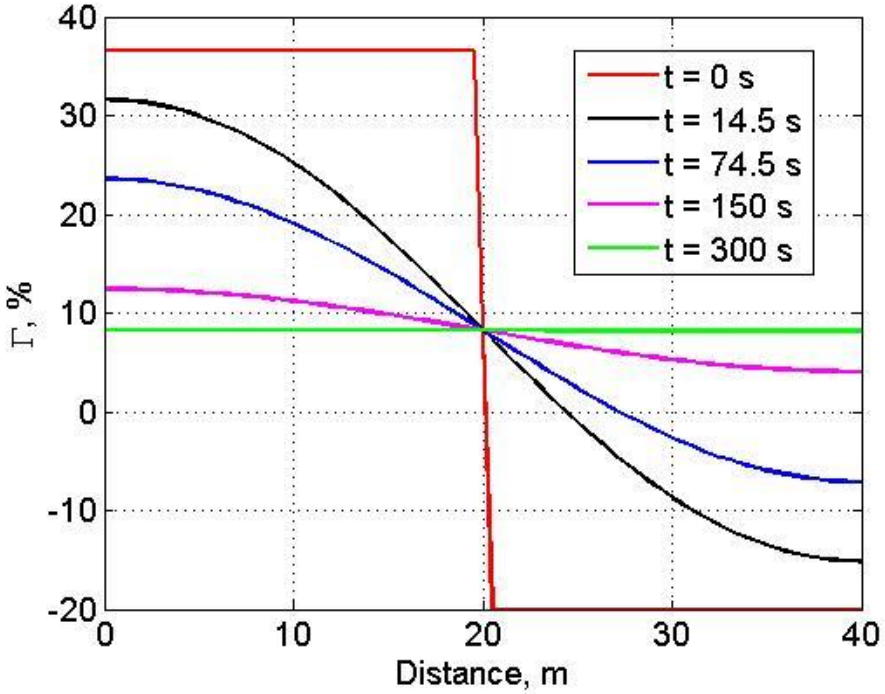

Fig. 2. An example of $\Gamma(x,t)$ evolution during mixing.

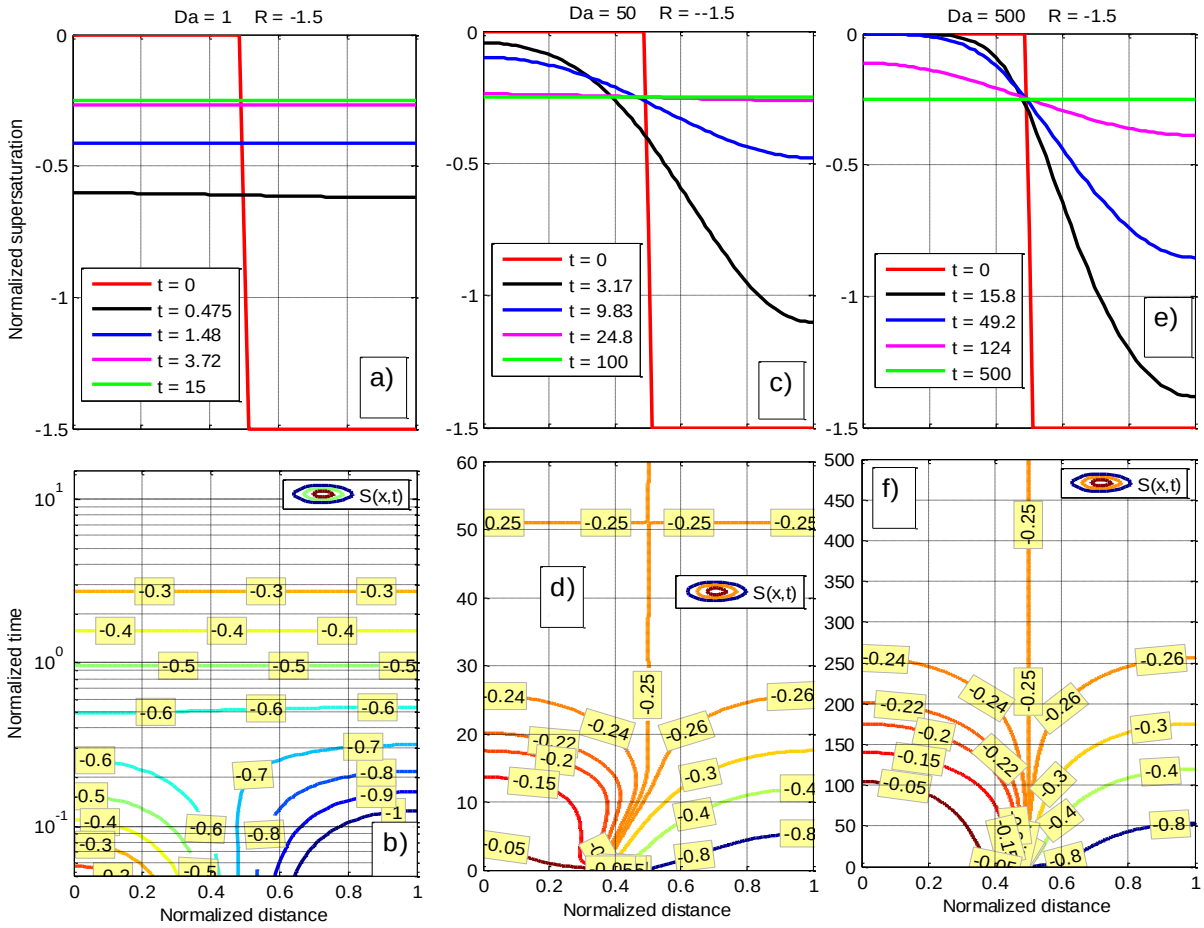

Fig. 3. Horizontal dependencies (upper row) and $\tilde{x}-\tilde{t}$ dependencies (lower row) of normalized supersaturation at $Da=1$, Da =50 and Da =500 and at $R=-1.5$. Panel b is plotted in semi-log scale.

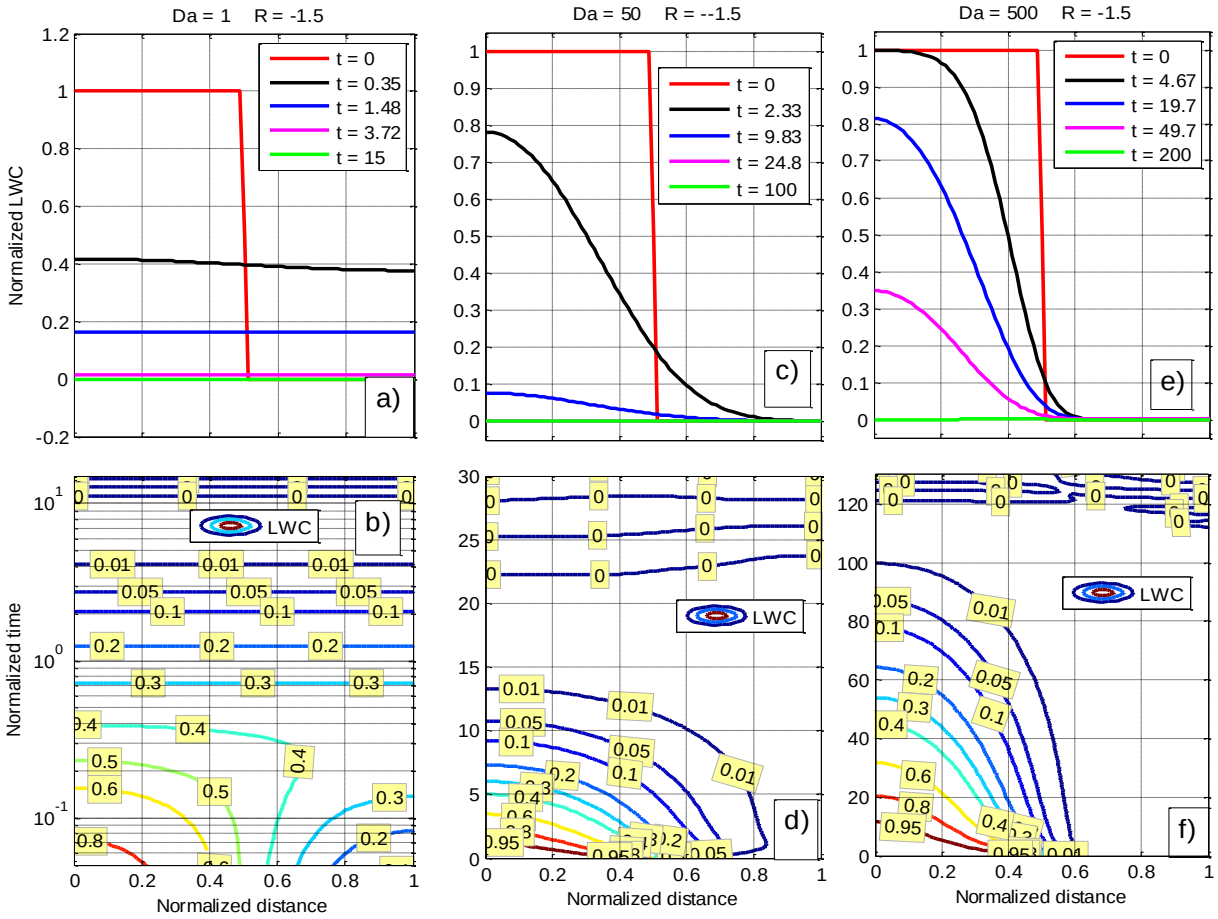

Fig. 4. The same as in Fig. 3, but for normalized LWC. Left bottom panel is plotted in semi-log scale.

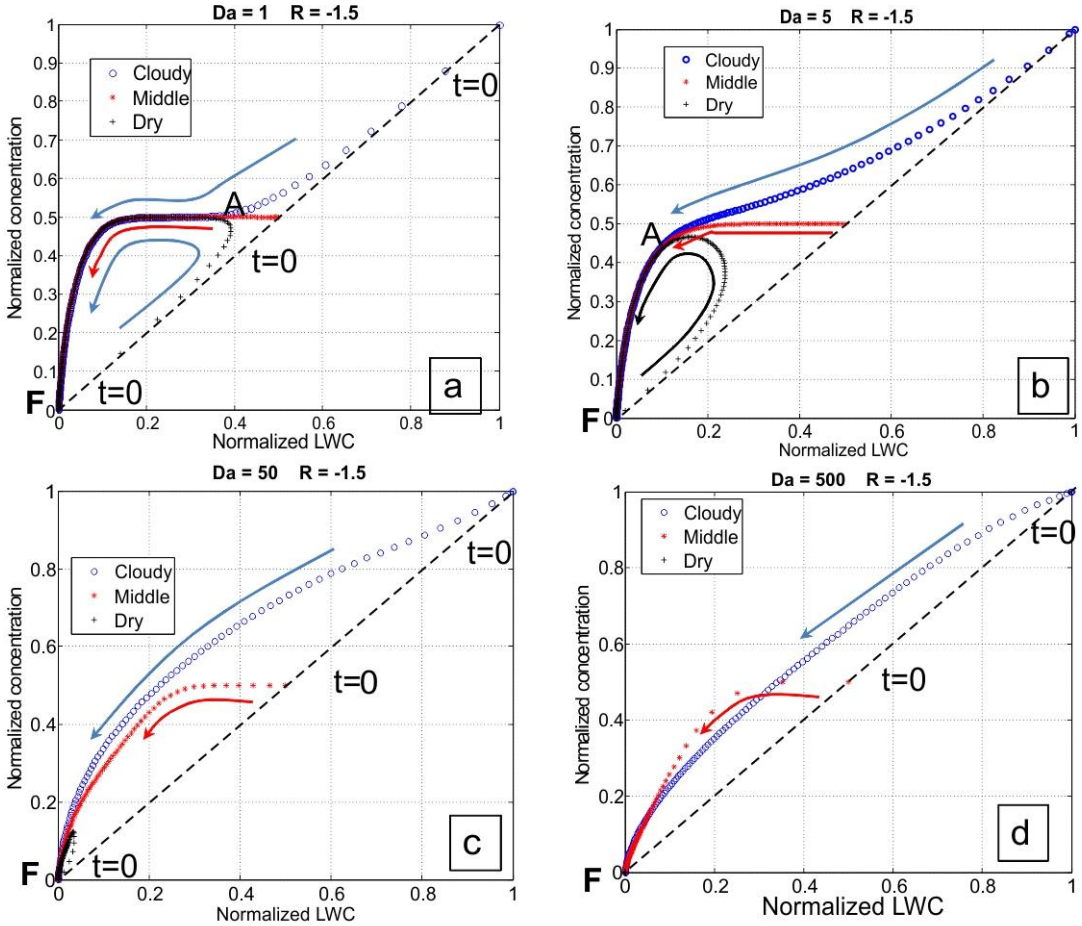

Fig. 5. Dependencies of normalized values of droplet concentration on normalized LWC at different Da and $R=-1.5$. Blue symbols mark the centre of the cloudy volume ($\tilde{x}=1/4$), red symbols mark the interface between the cloudy volume and the dry volume ($\tilde{x}=1/2$), and black crosses mark the centre of the initially droplet-free volume ($\tilde{x}=3/4$). Symbols are plotted at different time instances. Symbols at t=0 show initial values of droplet concentration and LWC at the three values of $\tilde{x}$. Arrows show the direction of movement of the points at the diagram with time. Point "A" marks the beginning of the spatially homogeneous stage, $\tilde{t}=T_{mix}$. Point "F" marks the final state. The dashed line indicates the relationship between $\tilde{N}$ and $\tilde{q}$ in extremely inhomogeneous mixing (according to the classical concept).

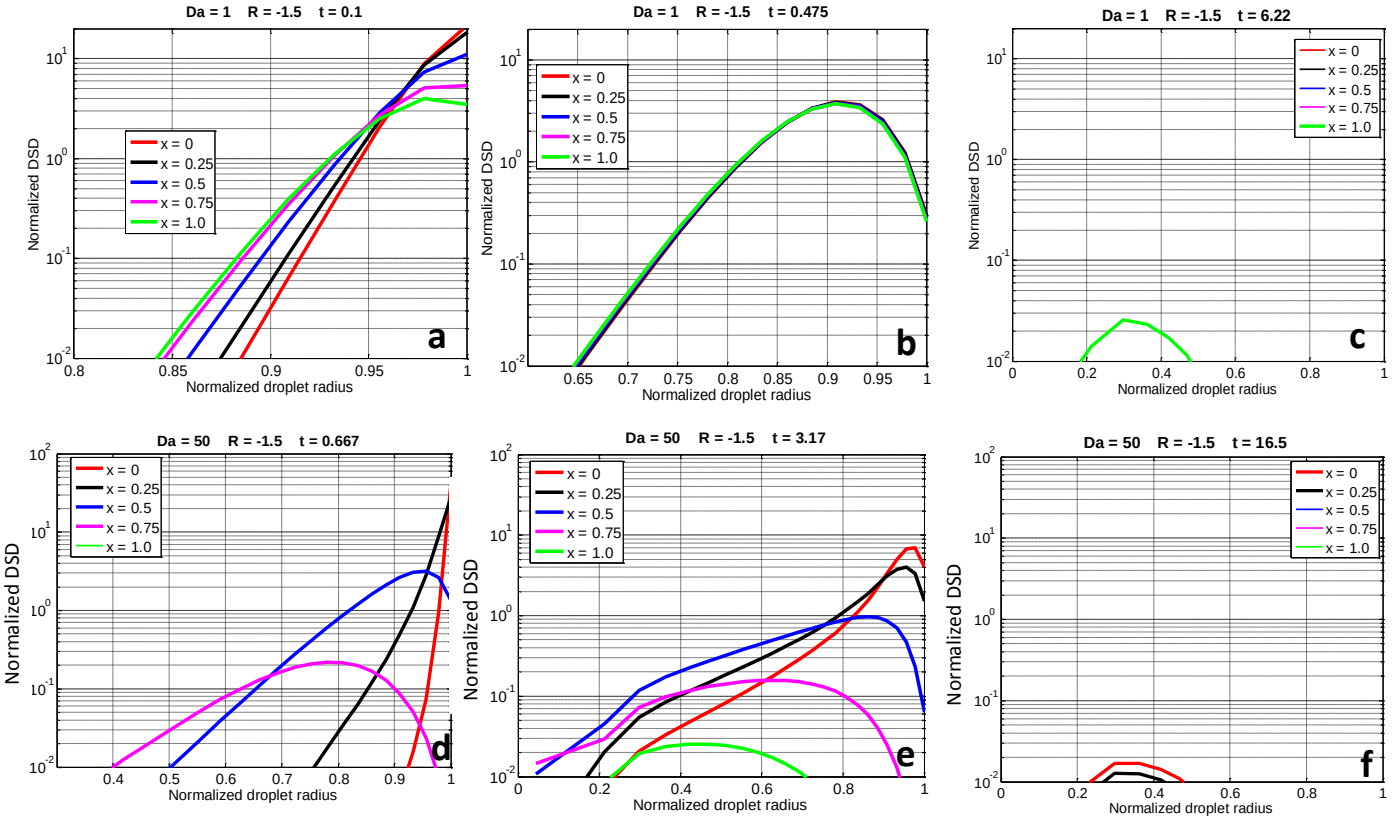

Fig. 6 Time evolution of DSD during droplet evaporation at $Da = 1$ (upper row) and $Da = 50$ (bottom row). In each panel, the normalized DSD are shown at different values of horizontal coordinate $\tilde{x}$. Different panels show DSD at different time instances.

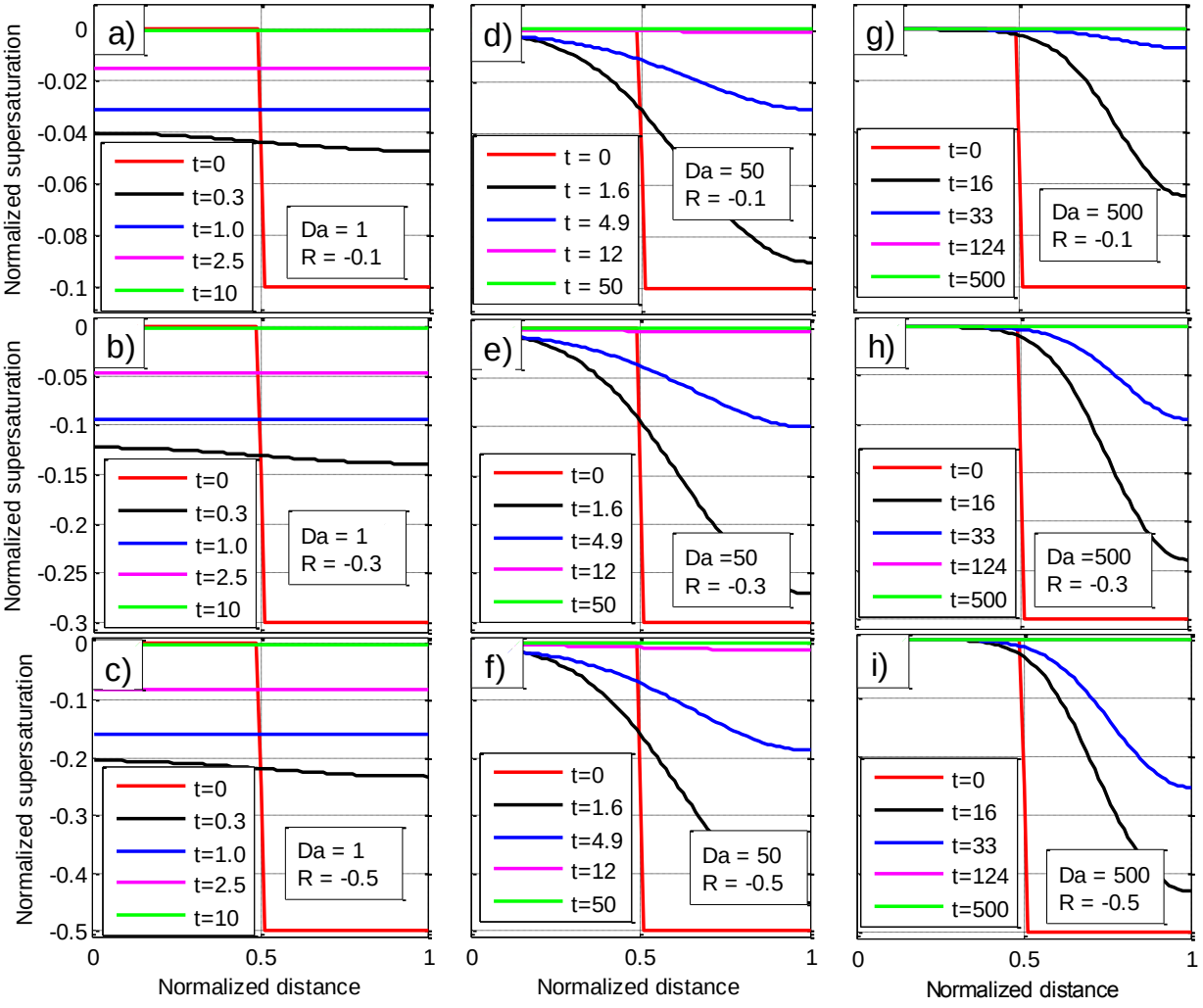

Fig. 7. Profiles of normalized supersaturation at different Da and different $R > -1$.

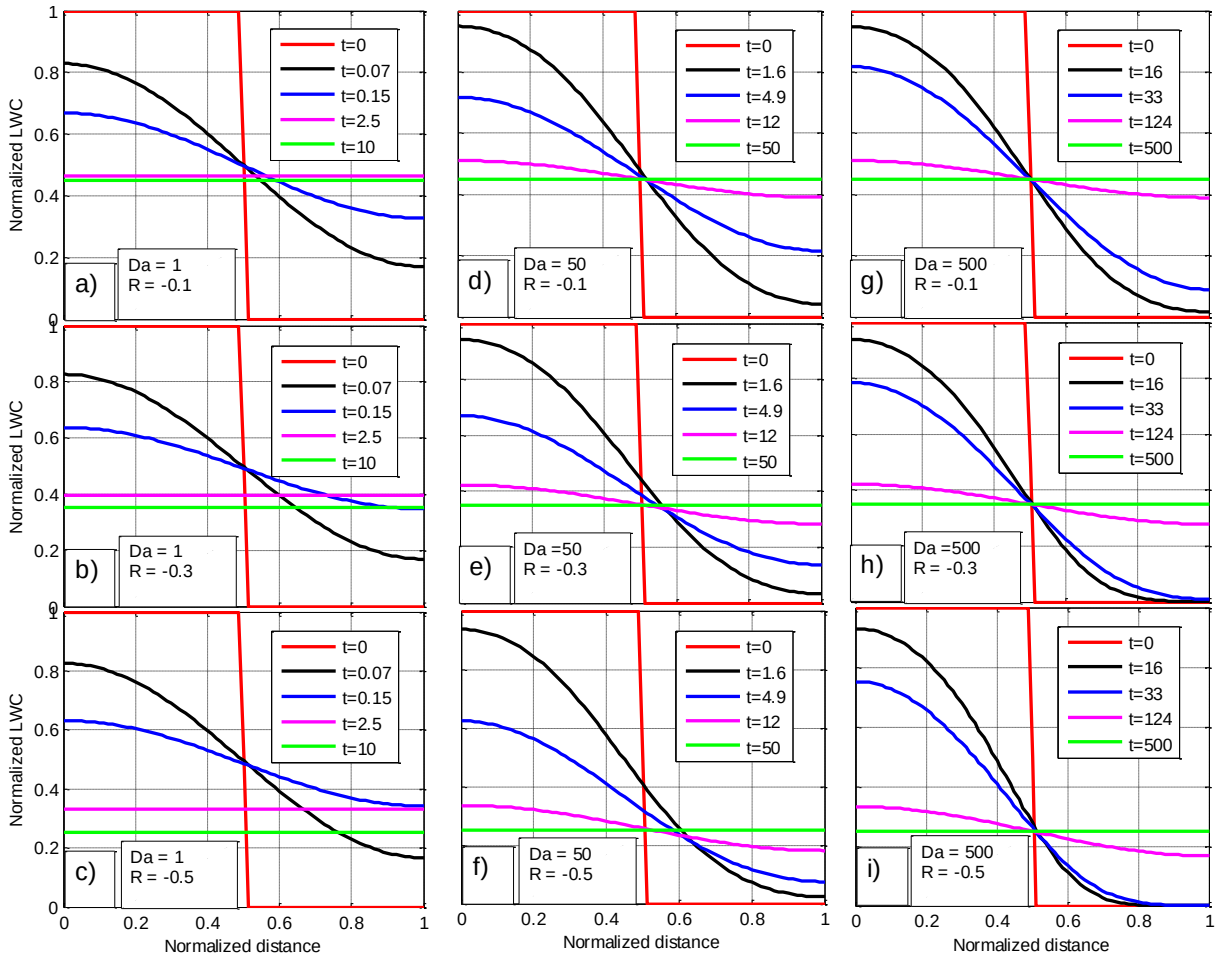

Fig. 8. Profiles of normalized LWC at different Da and at different $R > -1$.

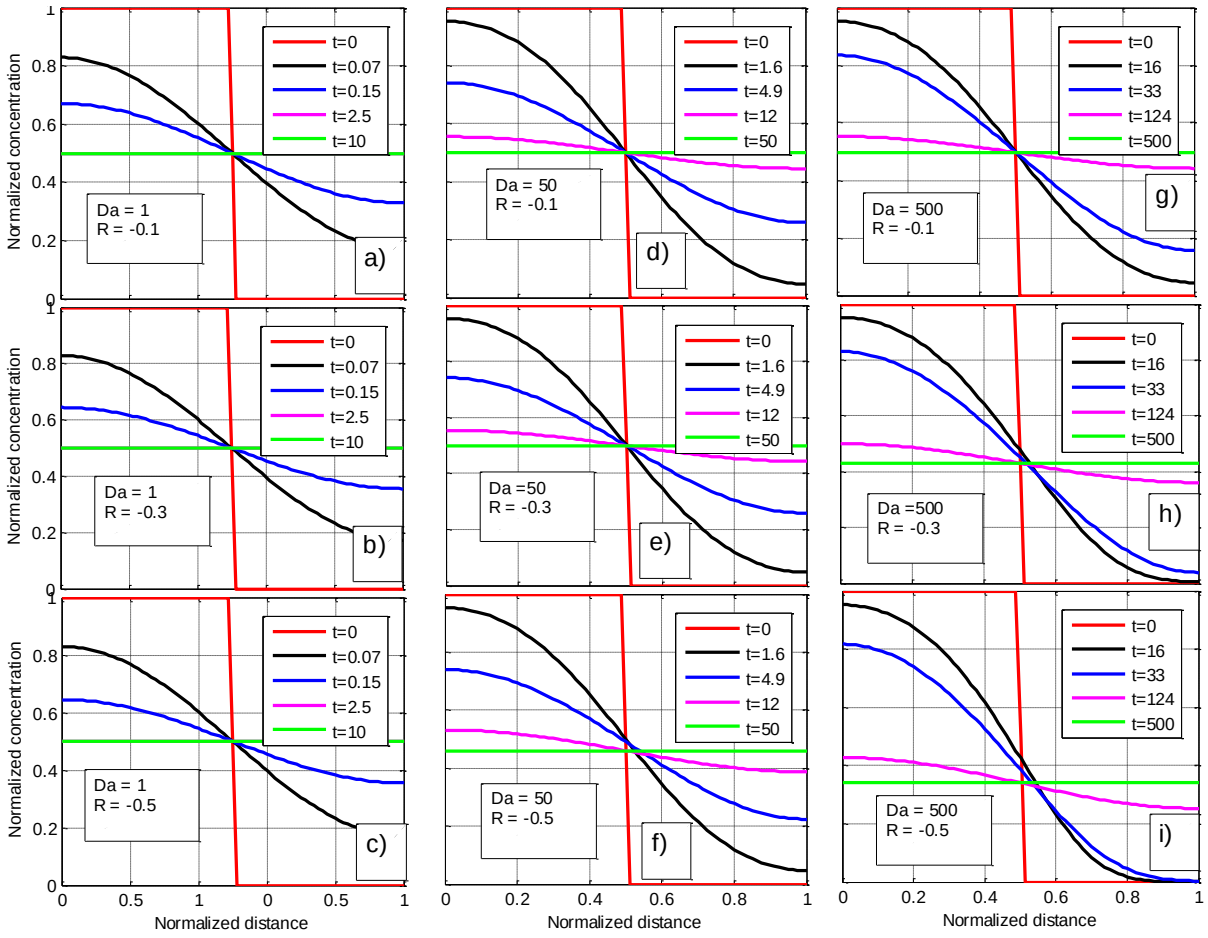

Fig. 9. Profiles of normalized droplet concentration at different Da and at different $R > -1$.

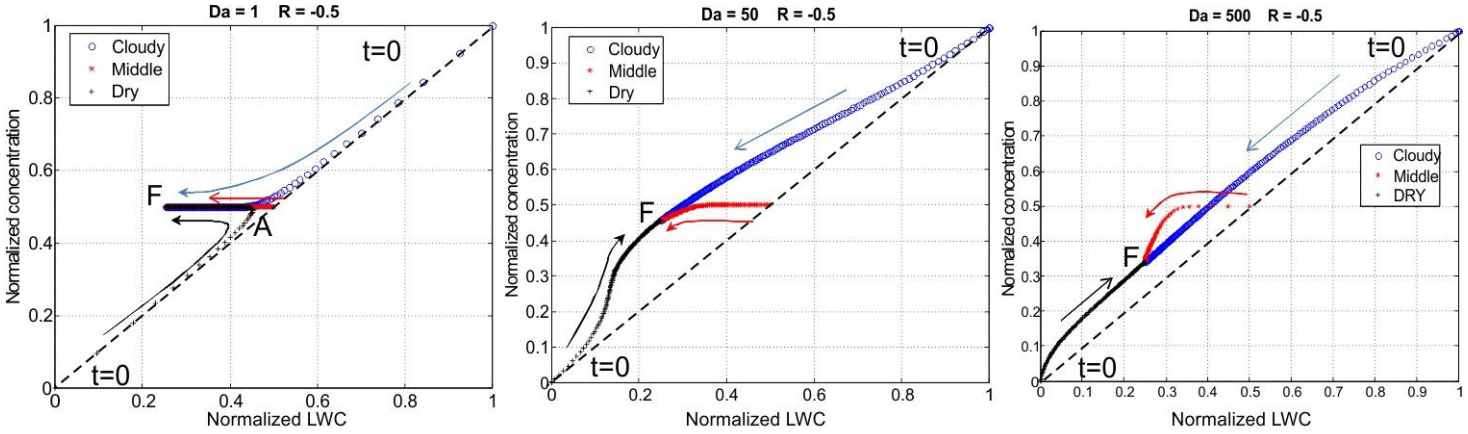

Fig. 10. Dependencies of normalized values of droplet concentration on normalized LWC at different *Da* and at $R = -0.5$. Blue circles mark the centre of the cloudy volume ($\tilde{x} = 1/4$), red symbols mark the initial interface ($\tilde{x} = 1/2$) and black crosses mark the centre of the initially dry volume ($\tilde{x} = 3/4$). Arrows show the direction of movement of the points with time. Point "F" marks the final stationary state of the system. The dashed line indicates the relationship between $\tilde{N}$ and $\tilde{q}$ in extremely inhomogeneous mixing (according to the classical concept).

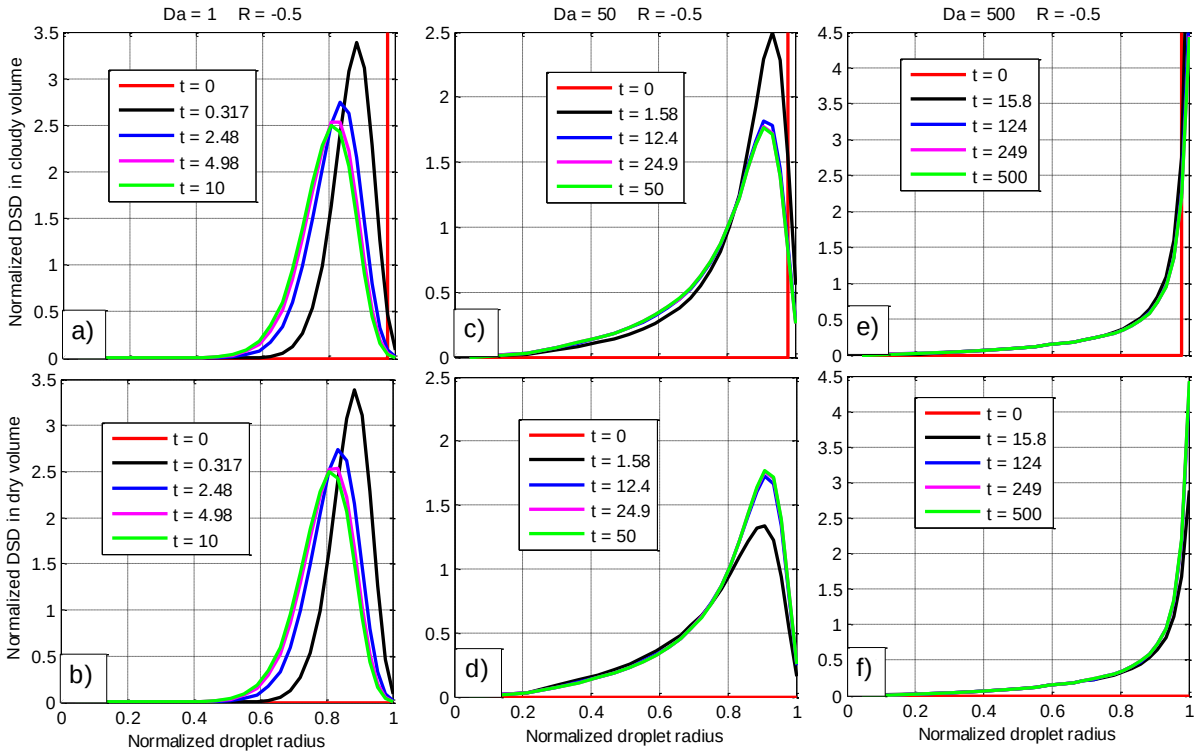

Fig. 11 Examples of DSD evolution in the initially cloudy volume ($\tilde{x}=1/4$) (upper row) and in the initially dry volume ($\tilde{x}=3/4$) (lower row) at $R=-0.5$ and at different values of Da.

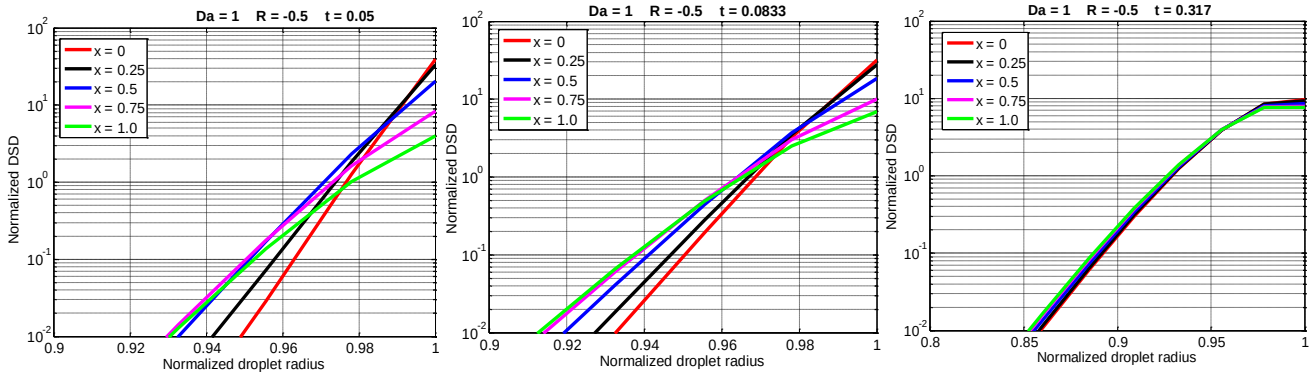

Fig. 12. DSD at different $\tilde{x}$ at the beginning of the mixing process for $Da = 1$ and $R = -0.5$.

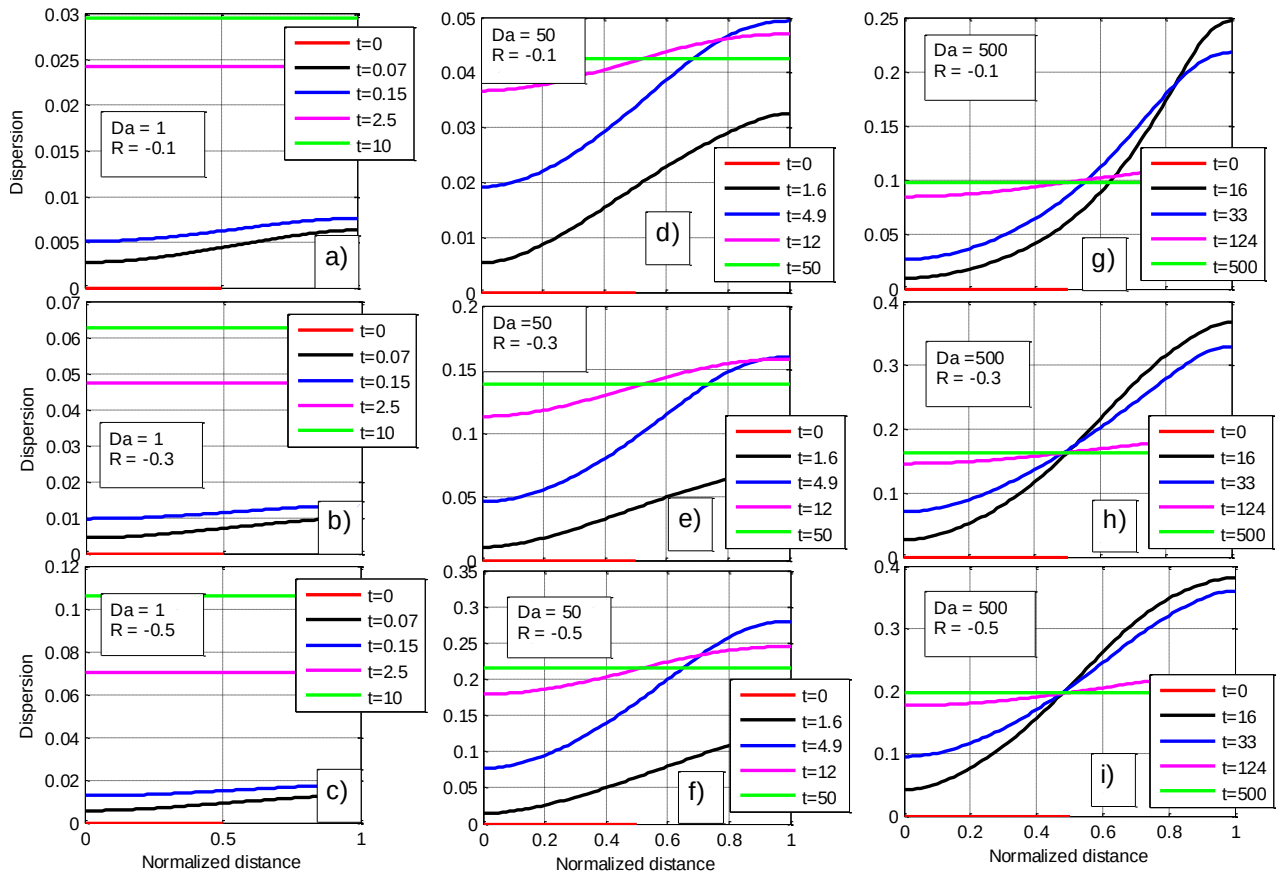

Fig. 13. Spatial dependencies of the relative DSD dispersion at different time instances and at different values of Da and different $R > -1$

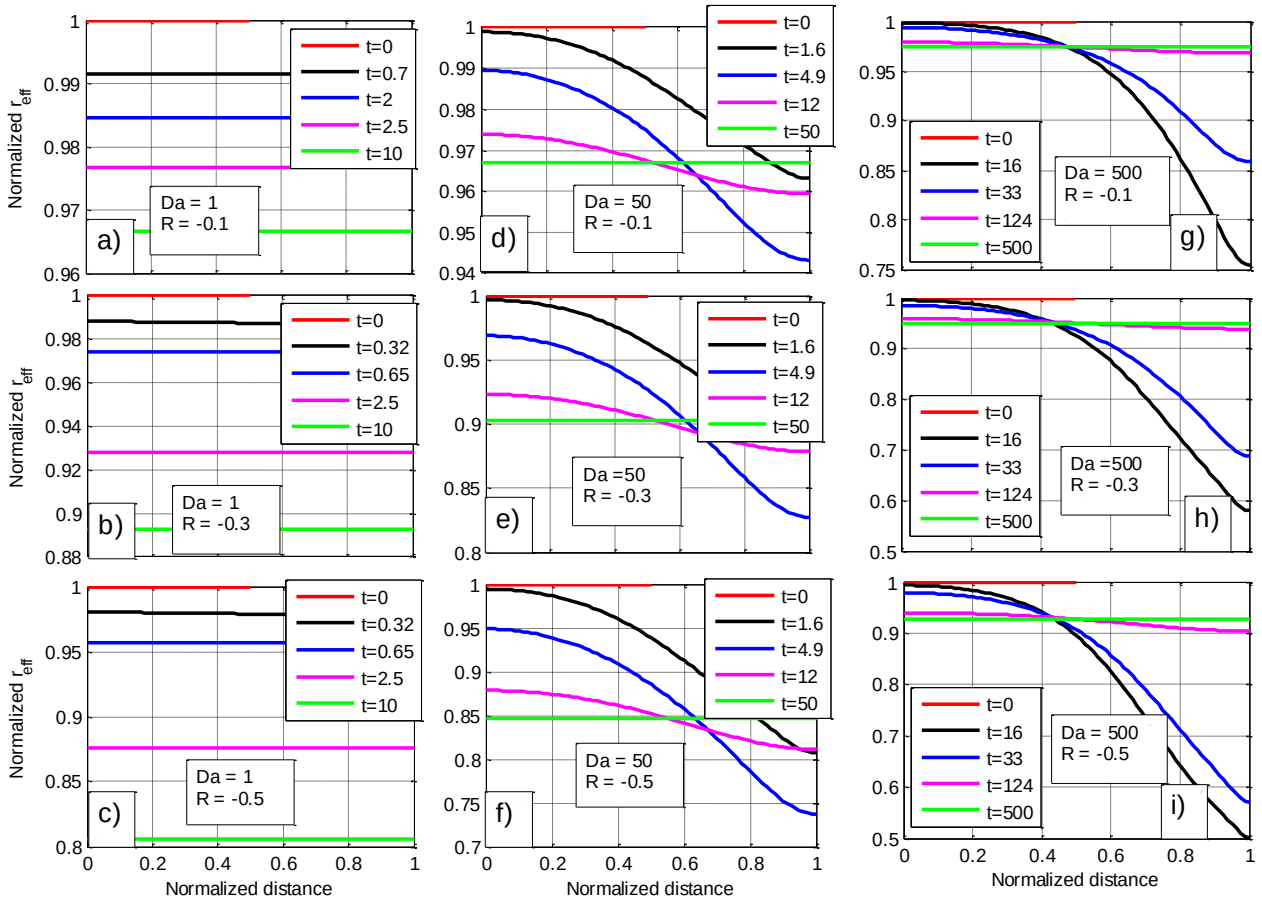

Fig. 14. Spatial dependencies of the effective radius at different time instances and at different values of Da and different $R > -1$

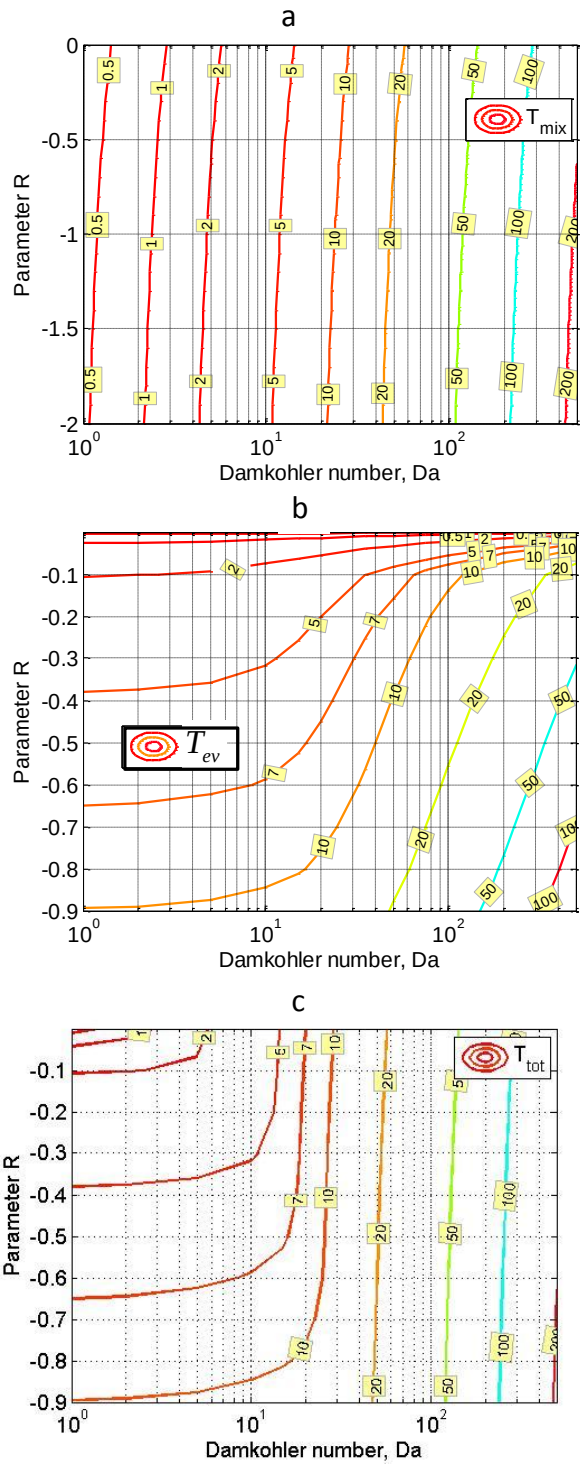

Fig. 15. Contours of normalized mixing duration times on $Da-R$ plane. (a) mixing time T_{mix}, (b) evaporation time T_{ev}, and (c) the total duration mixing time T_{tot}.

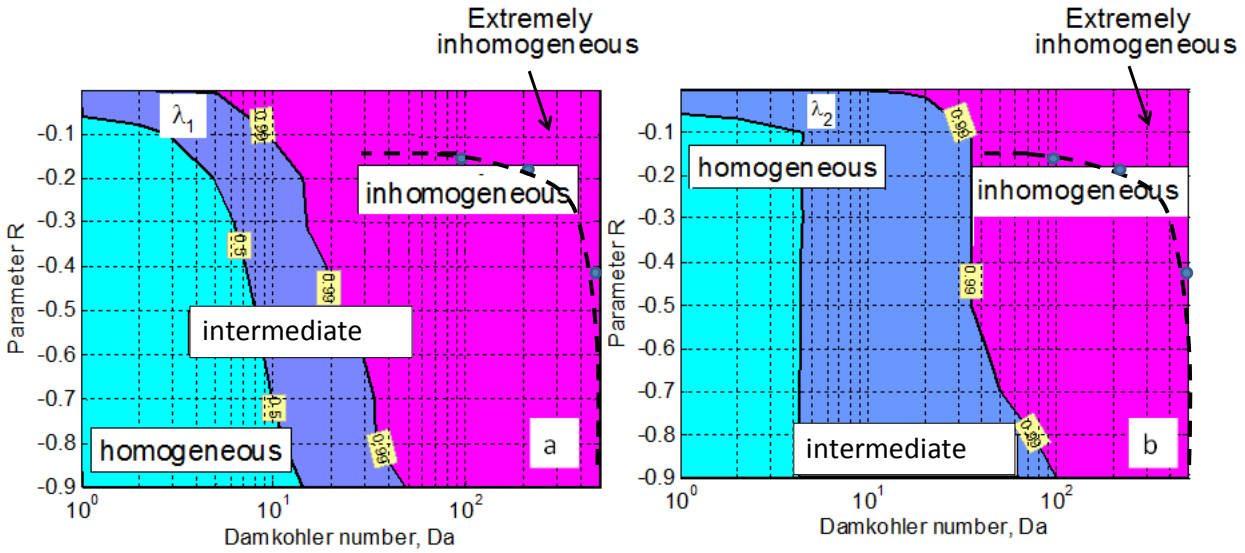

(a) **(b)**

Fig. 16. (a) The boundaries between mixing types on the $Da-R$ plane designed according to criteria $\lambda_1 = \frac{T_{mix}}{T_{tot}}$; **(b)** The boundaries between mixing types on the $Da-R$ plane designed according to criterion $\lambda_2 = \frac{2\langle \tilde{q}(T_{mix})\rangle - 1}{R}$ (Eq. 41). Dashed lines indicate the line corresponding to 2% deviation from the initial mean volume radius.

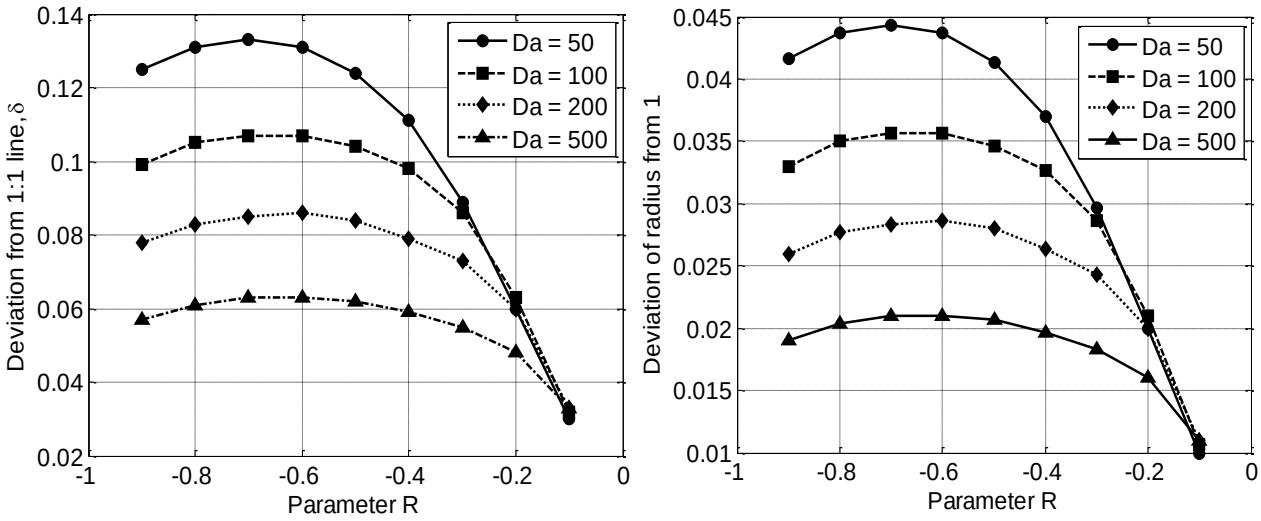

(a) (b)

Fig 17. (a) Dependencies of the r.m.s. distance of the $\tilde{N} - \tilde{q}$ relationship curve from straight line 1:1 suggested by classical concept of extremely inhomogeneous mixing. The dependencies are plotted for different values of Da and R. (b) The same as to the left panel but for r.m.s. deviations of the mean volume radius curve from that initial constant value assumed in the classical concept.